Journal of Marine Research, 70, 31–68, 2012

The air-sea transformation and residual overturning circulation within the Nordic Seas

by Pål Erik Isachsen[1] and Ole Anders Nøst[2]

ABSTRACT

The residual diapycnal overturning circulation through interior regions of the Nordic Seas is diagnosed. The mean flow is estimated from Ekman dynamics and from the thermal wind relation with reference level velocities deduced from observations and from simplified theory. Eddy-induced transport is estimated from a GM-type parameterization which includes top and bottom boundary layers. The contributions from the Eulerian mean and eddy-induced transport are then compared to the annual-mean air – sea density transformation over the Nordic Seas. The calculations suggest that the mean flow overturning may explain up to 25% of the observed air – sea transformation in the Lofoten-Norwegian Sea basins. But, over all, eddy-induced overturning must dominate the transport of buoyancy and heat into these interior regions, and the eddy parameterization used here is able to explain most of the density transformation rates. The calculations generally support previous claims that small-scale mixing is of secondary importance in high-latitude regions such as this, but they also open for the existence of a deep mixing-driven overturning cell between the eastern and western parts of the Nordic Seas.

1. Introduction

The east-west boundaries caused by continents allow the oceanic meridional heat transport to be mediated largely by time-mean geostrophic currents. The currents and their heat transport may, therefore, be quantified by the classic thermal wind method with some independent estimates of reference-level velocities (e.g. Ganachaud and Wunsch, 2003). The notable exception is the Southern Ocean: resembling mid-latitude atmospheric wind systems, the large-scale geostrophic currents of the Antarctic Circumpolar Current (ACC) are primarily zonal and unfit to transport much heat — thermal energy — poleward. The *residual* circulation that actually advects heat and other tracers meridionally there is primarily eddy-driven, caused by baroclinic instability of the mean zonal currents (de Szoeke and Levine, 1981; Döös and Webb, 1994; Karsten and Marshall, 2002; Marshall and Radko, 2003).

1. Norwegian Meteorological Institute, Oslo, Norway. ***email: palei@met.no***
2. Norwegian Polar Institute, Tromsø, Norway.

At high northern latitudes the meridional heat transport is dominated by time-mean boundary currents locked to the continental slopes, and it may appear that baroclinic instability and eddy-induced heat transport is of little importance. But mesoscale eddies do have a key role to play in the north as well. By spreading the heat laterally away from boundary currents and into the wider ocean basins, eddy transport increases the surface area over which the warm water is exposed to the atmosphere. At low latitudes baroclinic planetary Rossby waves can spread out the temperature signal of a warm boundary current. But in mid and high latitudes the planetary waves travel too slowly, and baroclinic instability and nonlinear eddy advection dominate (LaCasce and Pedlosky, 2004; Pedlosky and Spall, 2005; Isachsen *et al.*, 2007a). It has been shown, for example, that the oceanic heat loss to the atmosphere and the formation of dense waters in the Labrador Sea of the northwestern North Atlantic relies on (1) geostrophically-balanced boundary currents bringing warm waters into the region, and (2) eddy fluxes then spreading the heat over the Labrador Sea proper (Straneo, 2006a, and references therein).

There is much indication that the situation is similar in the Nordic Seas, another prime source of dense waters in the northeastern corner of the North Atlantic. Figure 1 shows the bottom bathymetry of the Nordic Seas along with the NCEP/NCAR CDAS-1 reanalysis (Kalnay *et al.*, 1996) estimate of the annual net heat loss to the atmosphere. The implied oceanic heat transport convergence in this marginal sea, about 140 TW in total, is essentially caused by the import of warm and salty Atlantic Water and export of colder and fresher waters across the Greenland-Scotland Ridge in the south. The warm Atlantic Water flows northward in various branches along the eastern margin while the cold return water flows southward in the west (see e.g. Mauritzen, 1996 and Segtnan *et al.*, 2011 for schematic descriptions of the large-scale currents). In our figure the heat loss to the atmosphere is also shown for three sub-regions within the Nordic Seas proper, and from this we can see that the heat loss over the interior regions deeper than 1250 m (labeled NSi in the figure) is nearly three quarters of the total. The important point to note here is that these interior regions are most likely shielded from significant large-scale water exchange with the surrounding oceans. The large-scale currents are heavily guided by the ambient potential vorticity field, f/H (where f is the Coriolis parameter and H the bottom depth), and the overwhelming influence of topography at high northern latitudes creates 'closed-f/H' basins that do not connect to the North Atlantic Ocean across the Greenland-Scotland Ridge.

Strictly speaking it is only the bottom geostrophic flow which, to lowest order, needs to follow f/H contours. In a rotating stratified fluid the orientation of the geostrophic flow may change with height given nonzero vertical mean velocities or ageostrophic mixing of density (Schott and Stommel, 1978; Schott and Zantopp, 1980). A theoretical possibility therefore exists that geostrophic currents higher in the water column cross contours of f/H and that some percentage of the total heat flux into these interior regions is carried by the large-scale currents. And yet observations show that most of the surface currents in the region also tend to follow topography. In recent years it has therefore become generally

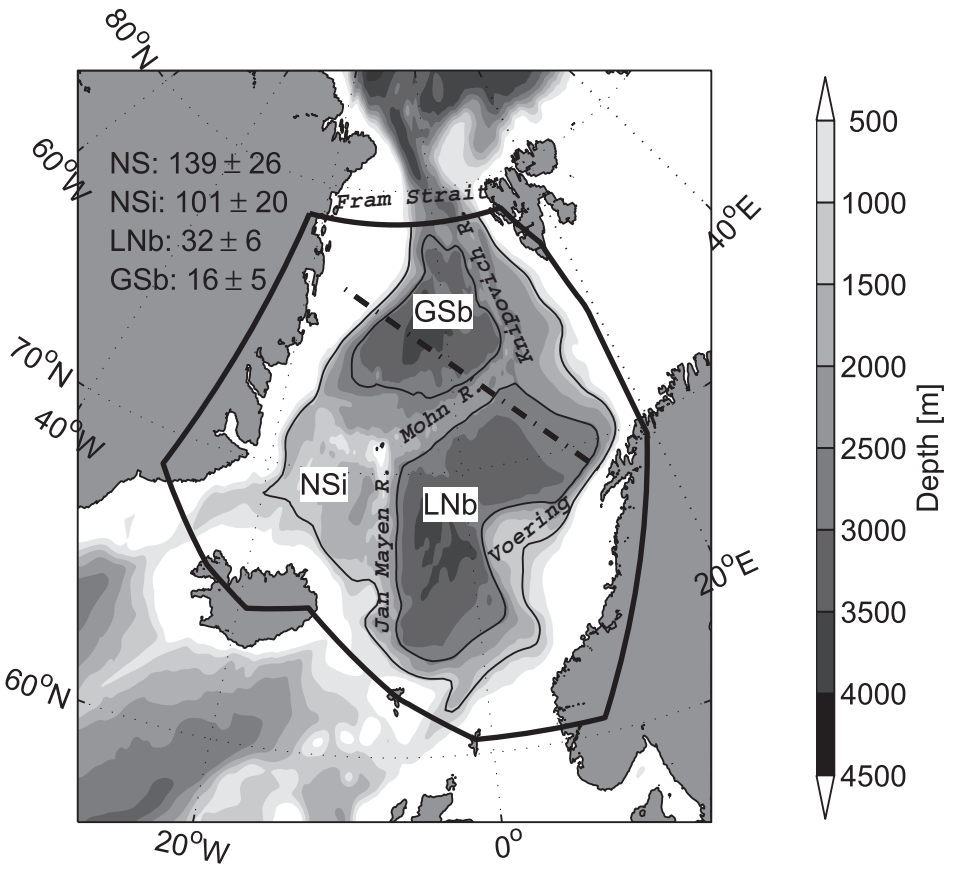

Figure 1. The Nordic Seas (defined by the thick line) with three interior regions traced out by thinner lines: NSi = Nordic Seas interior which also includes LNb = Lofoten and Norwegian basins, and GSb = Greenland Sea basin. A dash-dot line shows a transect discussed in the text. Estimates of the annual net heat loss (in TW) from the NCEP-NCAR CDAS-1 reanalysis is also shown.

accepted that lateral mesoscale eddy fluxes are of crucial importance to the oceanic heat loss and dense water formation that takes place in the Nordic Seas.

A series of idealized theoretical studies and numerical simulations by Spall (2004, 2005, 2010a,b) have all supported this picture. The studies have all been cast in terms of generic marginal seas but have been motivated by the situation in the Nordic Seas and Labrador Sea. The collective work has illuminated how mean-flow advection is limited to the boundary currents and how the total air-sea heat flux is intimately tied to lateral eddy heat transport away from these boundary currents. Intended to develop our intuition about these processes, the models have necessarily been extremely crude idealizations of the real world. We now believe the situation in the Nordic Seas needs to be assessed from actual observations.

In this paper we utilize a range of gridded data combined with simplified theory to try to close the buoyancy budgets (more specifically, the potential density budgets) for the large interior basins of the Nordic Seas. The air-sea heat flux is really the quantity of direct relevance for the atmospheric climate, but over large parts of the Nordic Seas buoyancy is a good proxy for temperature, especially east of the Jan Mayen-Mohn-Knipovich (JMK) Ridge. More importantly, it is buoyancy which is of direct dynamical relevance to the ocean overturning circulation itself. In the following, air-sea fluxes and the air-sea density transformation will be estimated from two atmospheric reanalysis products and from a new hydrographic climatology of the Nordic Seas. Estimates of the time-mean transport will rely on the calculation of Ekman flows and thermal wind currents with either assumptions for, or observations of, the reference-level velocities. Finally, estimates of the mesoscale eddy transports will be based on a state-of-the-art parameterization of eddy-induced overturning.

2. Methods and data

a. The Walin framework in an eddying ocean

The framework linking the water mass transformation by diabatic density fluxes to the diapycnal overturning circulation was originally laid out by Walin (1982) and later elaborated by numerous others (e.g. Garret and Tandon, 1997; Nurser *et al.*, 1999; Marshall *et al.*, 1999). A brief summary of the framework and its interpretation in an eddying ocean—using Transformed Residual Mean (TRM) theory—is given below.

Consider a control volume consisting of waters below (denser than) some neutral density surface or isopycnal σ' within one of our sub-regions in Figure 1. The volume V evolves according to (see Fig. 2):

$$\frac{\partial V}{\partial t} = G - M, \tag{1}$$

where G is the total light-to-dense diapycnal transport through σ' and M is the total horizontal transport of waters denser than σ' out of the control volume. Specifically, if s is the horizontal coordinate along a contour defining our subregion and $\hat{\mathbf{n}}$ is the outward-pointing unit vector normal to the contour, then

$$M = \oint \mathbf{U}(s) \cdot \hat{\mathbf{n}}\, ds, \tag{2}$$

where $\mathbf{U}$ is the transport per unit horizontal distance under σ' at each position, i.e.

$$\mathbf{U}(s) = \int_{-H(s)}^{z_{\sigma'}(s)} \mathbf{u}(s, z)\, dz, \tag{3}$$

for velocity vector $\mathbf{u}$, bottom depth H ($H > 0$) and z-level ($z_\sigma \leq 0$) of isopycnal σ'. The diapycnal volume transport G through σ' is found by considering volume and potential density conservation within a second infinitesimal control volume between σ' and $\sigma' + \Delta\sigma$.

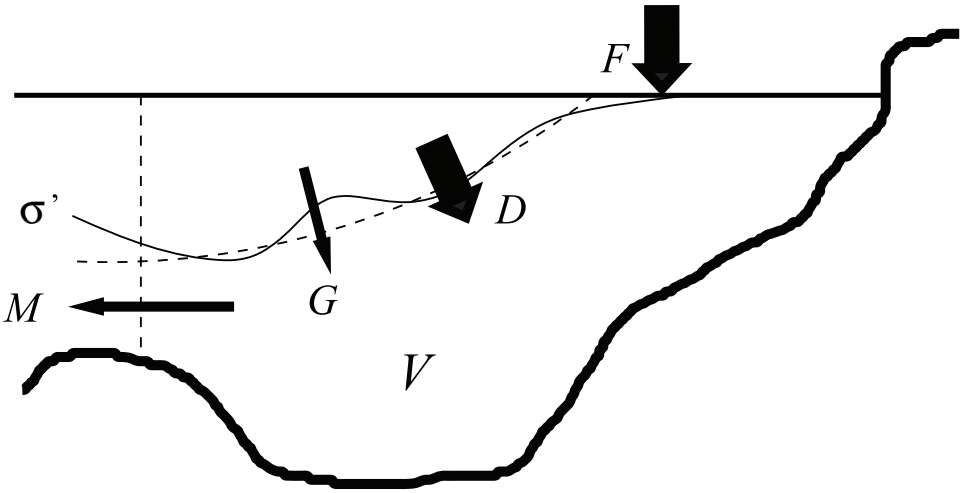

Figure 2. The volume budget for waters denser than a given potential density σ' within an enclosed ocean region. The time evolution of volume V is given by the light-to-dense diapycnal volume transport G through isopycnal σ' minus the lateral transport M of waters denser than σ' out of the region. The diapycnal volume transport G is set by the net air-sea density flux F and the convergence of turbulent diabatic density fluxes $-\partial D/\partial\sigma$ on σ'. The thin solid line indicates an instantaneous position of σ' while the dashed line is the mean depth when averaged over some eddy mixing time scale.

The derivation has been given in numerous previous studies (see e.g. Marshall *et al.*, 1999) and the central result can be written as

$$G = F - \frac{\partial D}{\partial \sigma}. \tag{4}$$

Here $-\partial D/\partial\sigma$ is the instantaneous convergence of small-scale turbulent diapycnal density fluxes on σ' (including contributions from quasi-horizontal mixing in the surface layer, mixing at the base of this surface layer and quasi-vertical mixing in the ocean interior; see section 3b below) and F is the instantaneous air-sea density flux on σ', the so-called *air-sea transformation* of density on σ'. In practice, this air-sea transformation is found by integrating the air-sea density flux f_σ over the infinitesimal outcrop area between isopycnals σ' and $\sigma' + \Delta\sigma$ and then dividing by $\Delta\sigma$,

$$F(\sigma') = \lim_{\Delta\sigma\to 0} \frac{1}{\Delta\sigma} \iint_{\sigma'}^{\sigma'+\Delta\sigma} f_\sigma \, dA. \tag{5}$$

One may think of the operation as a mapping of the air-sea density fluxes from geographic coordinates to density coordinates.

We now integrate both (1) and (4) over some characteristic eddy mixing time scale[3] while all the time *following the movement of isopycnal* σ'. The resulting balances may be written

$$\frac{\partial \hat{V}}{\partial t} = \hat{G} - \hat{M} \tag{6}$$

$$\hat{G} = \hat{F} - \widehat{\frac{\partial D}{\partial \sigma}}, \tag{7}$$

or, combining,

$$\frac{\partial \hat{V}}{\partial t} = \left(\hat{F} - \widehat{\frac{\partial D}{\partial \sigma}} \right) - \hat{M}, \tag{8}$$

where the hat over each variable indicates that the time average was made following the movement of the isopycnal. Specifically, $\hat{M}$ is the time-mean horizontal transport of waters denser than σ' out through the transect. And since, by continuity, $\hat{M}$ is also the time-mean transport of waters lighter than σ' into the control volume, it represents the time-mean overturning transport evaluated in density coordinates.

Next, the Temporal Residual Mean framework (TRM; McDougall and McIntosh, 2001) shows how $\hat{M}$ may be written in terms of time-mean transports that are instead evaluated at fixed height. The time-mean transport under σ' per unit length may be written

$$\hat{\mathbf{U}} = \overline{\mathbf{U}} + \mathbf{U}^{\#} \equiv \overline{\mathbf{U}}^{\#}, \tag{9}$$

where $\overline{\mathbf{U}}^{\#}$, the TRM transport streamfunction, is the sum of the Eulerian mean streamfunction $\overline{\mathbf{U}}$ and the eddy-induced streamfunction $\mathbf{U}^{\#}$, both *evaluated at the time-mean height* $\hat{z}_{\sigma'}$ *of the isopycnal*. The advantage of this form is that the Eulerian time mean flow (which we shall assume is resolved by the data) and the eddy transport (which must be parametrized) are usually both more easily evaluated at fixed height rather than at fixed potential density. Integrating around a closed contour as in (2) gives

$$\frac{\partial \hat{V}}{\partial t} = \hat{F} - \widehat{\frac{\partial D}{\partial \sigma}} - \{\overline{M} + M^{\#}\}. \tag{10}$$

Finally, we also integrate over the seasonal cycle since we expect annual-mean volume changes to be small compared to the advective throughflow. The approximate annual-mean balance then becomes

$$\langle \overline{M} \rangle + \langle M^{\#} \rangle \simeq \langle \hat{F} \rangle - \left\langle \widehat{\frac{\partial D}{\partial \sigma}} \right\rangle, \tag{11}$$

3. We will leave out the issue of characteristic eddy length scales even though this is clearly an issue of equal importance.

where the angle brackets indicate an average over times longer than the eddy correlation time scales and up to one year (or over several whole years). It should be observed that the derivative of this expression with respect to density,

$$\frac{\partial}{\partial\sigma}(\langle\overline{M}\rangle + \langle M^{\#}\rangle) \simeq \frac{\partial}{\partial\sigma}\left(\langle\hat{F}\rangle - \left\langle\widehat{\frac{\partial D}{\partial\sigma}}\right\rangle\right), \tag{12}$$

gives an indication of the direction of the diapycnal overturning flow, or 'thickness flux,' at any given density. Here it is useful to again recall that $\overline{M}^{\#} = \overline{M} + M^{\#}$ is the total transport of waters out of the control volume, integrated from the bottom and up to time-mean height $\hat{z}_{\sigma'}$, but also, because of continuity, the transport of waters into the control volume, integrated from the surface and down to $\hat{z}_{\sigma'}$. Thus, $\partial\overline{M}^{\#}/\partial\sigma > 0$ means that the transport streamfunction for flow into the domain, referenced to the surface, increases with density (or, alternatively, that the transport streamfunction for flow out of the domain, referenced to the bottom, decreases with density), meaning a net import of water. Thus, given that volume changes are negligible, if the total transformation at any given density (the right-hand side of 12) increases with density, i.e. if the transformation curve has a positive slope, there must also be a net flow into the domain at this density. Conversely, a negative slope of the transformation curve indicates a net outflow.

Note in closing that an alternative path to these final expressions exists. One may first cast the buoyancy equation into residual form (where the total advection velocity is written as a sum of an Eulerian mean and an eddy-induced velocity) and then proceed to make the above integral budgets on the time-mean density field (see e.g. Marshall and Radko, 2003).

In this study we will assume that eddy correlations are important up to time scales of one month. The discrete version of (11) then becomes

$$\frac{1}{12}\sum_{m=1}^{12}\overline{M}_m + \frac{1}{12}\sum_{m=1}^{12}M^{\#}_m \simeq \frac{1}{12}\sum_{m=1}^{12}\hat{F}_m - \frac{1}{12}\sum_{m=1}^{12}-\widehat{\frac{\partial D}{\partial\sigma}}_m, \tag{13}$$

which is the expression to be evaluated in this study. Eulerian mean transport streamfunctions will be constructed from gridded observations of wind and hydrography, along with a simplified model for, or direct observations of, the bottom reference-level velocities. Streamfunctions for the eddy-induced flow will be based on a modern parameterization that includes top and bottom boundary layers. Since we lack observations of the correlations between air-sea fluxes and surface density field at sub-monthly time scales, the air-sea transformation will be calculated from monthly-mean heat and freshwater fluxes and monthly-mean surface hydrography. Finally, drawing on the conclusions of several earlier studies (Speer, 1997; Large and Nurser, 2001; Isachsen *et al.*, 2007b), we begin by assuming that convergent turbulent diapycnal density fluxes $-\partial D/\partial\sigma$ are of secondary importance in the annual-mean budget at high latitudes (but see a discussion of this issue later). So the question we ask is: How much of the annual-mean air-sea density transformation over the

interior regions of the Nordic Seas is tied to the Eulerian mean versus the eddy contribution to the total residual overturning circulation?

b. Air-sea transformation

As outlined in the Introduction, we will study the buoyancy budget for the three interior regions of the Nordic Seas shown in Figure 1. We define the *Nordic Seas interior* (NSi) as the region within the 1250 m depth contour except for a zonal stretch at 78°50′N in the Fram Strait between Greenland and Svalbard. The NSi subregion can thus communicate with the Arctic Ocean via the Fram Strait, but, as mentioned earlier, we expect access to the primary heat reservoir of the North Atlantic to be severely restricted. Within the NSi box there is also the *Lofoten-Norwegian Sea basins* (LNb) and the *Greenland Sea basin* (GSb) which we have here defined by 2500 m and 2750 m depth contours, respectively. These are interior basins that should be well shielded from advection by large-scale currents and the thermal energy carried by the Norwegian Atlantic Current.

The annual-mean air-sea density transformation will be estimated from monthly data as

$$\langle \hat{F} \rangle = \frac{1}{12} \sum_{m=1}^{12} \left\{ \lim_{\Delta\sigma \to 0} \frac{1}{\Delta\sigma} \int_{\sigma'}^{\sigma'+\Delta\sigma} f_\sigma \, dA \right\}_m , \tag{14}$$

i.e. by integrating air-sea density fluxes on a given isopycnal σ' each month and then following the movement of σ' from month to month. The density flux through the sea surface is calculated as (e.g. Marshall *et al.*, 1999)

$$f_\sigma = -\frac{\alpha}{c_p} Q + \rho_{S=0} \beta (-FW) S, \tag{15}$$

for heat and freshwater fluxes Q and FW (positive into the ocean), thermal expansion and haline contraction coefficients α and β, heat capacity c_p (all functions of surface salinity S and temperature T) and the density of freshwater $\rho_{S=0}$. Two different atmospheric reanalyzes were used to estimate fluxes: monthly mean NCEP/NCAR CDAS-1 (Kalnay *et al.*, 1996) at about 1.9 degree resolution (covering 1949–2010) and monthly mean ECMWF ERA-interim (Dee *et al.*, 2011) at 1.5 degree resolution (covering 1989–2009). The salinities, temperatures and densities used in these calculations, and also to be used later for estimating lateral transports at depth, were taken from a gridded monthly mean temperature and salinity climatology of the Nordic Seas made at about 50–70 km resolution (see Appendix A).

Figure 3 shows estimates of the annual-mean surface transformation for the entire Norwegian Sea and for the region within the 1250 m depth contour (NSi). The sign convention is such that positive $\langle \hat{F} \rangle$ indicates creation of denser water masses by air-sea fluxes. Also, as discussed in the previous section, if both small-scale turbulent mixing and volume changes are indeed unimportant, a positive slope ($\partial \langle \hat{F} \rangle / \partial\sigma > 0$) indicates a net flow of waters into the domain while a negative slope indicates a net export. The calculation thus traces

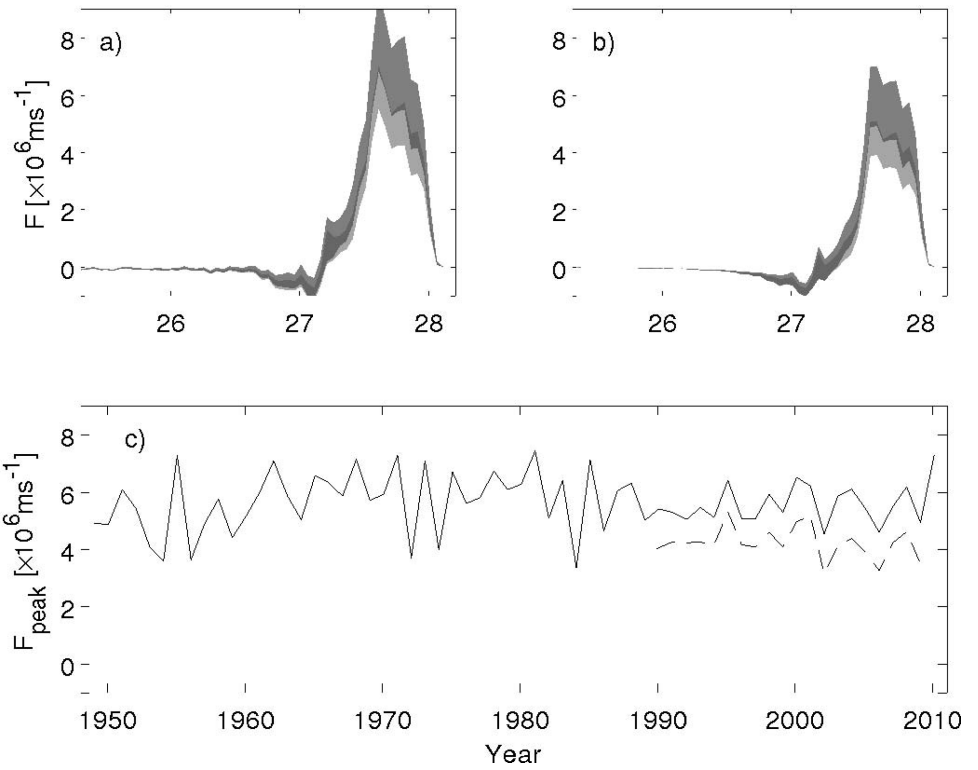

Figure 3. Annual net air-sea density transformation $\hat{F}$ over (a) the entire Nordic Seas and (b) the Nordic Seas interior box (NSi). Estimates are made from the CDAS-1 reanalysis (dark shading) and the ERA-interim reanalysis (light shading; very dark shading indicates the overlap). Means and standard deviations are taken over the reanalysis time periods (1949–2010 for CDAS-1 and 1989–2009 for ERA-interim). Also (c) the year-to-year estimates of average 'peak transformation' $\hat{F}_{peak}$ between $27.6 \leq \sigma_0 < 27.8\,\mathrm{kg\,m^{-3}}$ over NSi from CDAS-1 (solid line) and ERA-interim (dashed line).

out our common understanding of what takes place in the Nordic Seas: The region is dominated by the import of light waters and transformation to denser waters which are then exported. The CDAS-1 estimate of the peak transformation of waters in the range $27.6 \leq \sigma_0 < 27.8\,\mathrm{kg\,m^{-3}}$ is systematically about 20% higher than the ERA-interim estimate, and we should include this difference in our overall sense of uncertainties involved. But both reanalysis products confirm the picture derived from heat fluxes alone, namely that most of the air-sea density flux[4] and water mass transformation takes place within the interior regions of the Nordic Seas. We expect that these regions are effectively shielded from the reach of the mean flow, but this is precisely the issue to be addressed more carefully in the following.

4. The total air-sea density flux over the region is the area under the transformation curve.

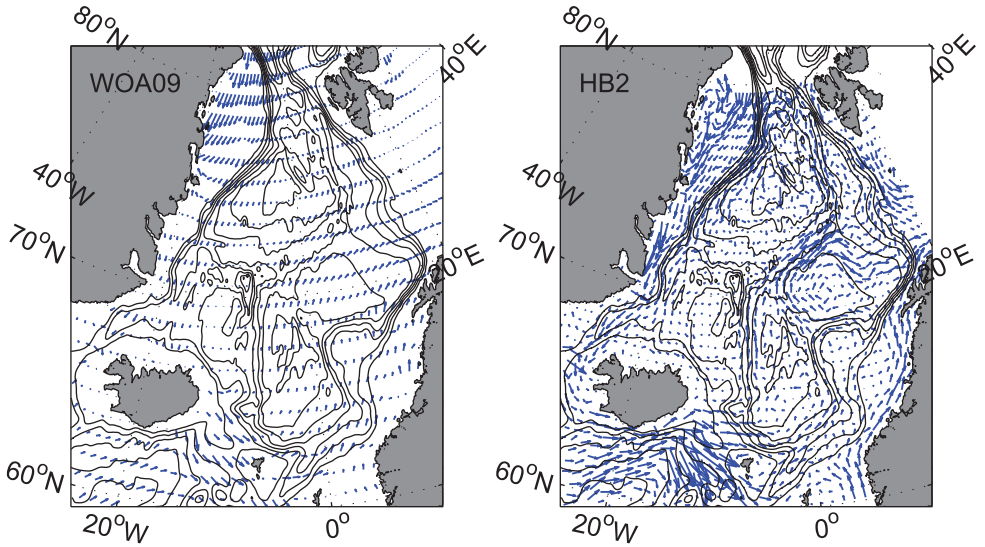

Figure 4. Annual-mean thermal wind currents relative to the bottom for (left) WOA09 and (right) the new "HB2" climatology. The scale of the arrows is arbitrary but the same for the two panels.

c. Eulerian mean transport

The Eulerian mean transport per unit length out of the control volume in Figure 2, i.e. the time-mean flow out below isopycnal σ', consists of the geostrophic transport and the surface and bottom Ekman transport. If all transports are integrated from the bottom and up to time-mean height $\hat{z}_{\sigma'}$, we can write:

$$\overline{\mathbf{U}}(\hat{z}_{\sigma'}) \cdot \hat{\mathbf{n}} = [\mathbf{U}_{tw}(\hat{z}_{\sigma'}) + (\hat{z}_{\sigma'} + H)\mathbf{u}_{ref}] \cdot \hat{\mathbf{n}} + \mathbf{U}_{E,s}(\hat{z}_{\sigma'}) \cdot \hat{\mathbf{n}} + \mathbf{U}_{E,b}(\hat{z}_{\sigma'}) \cdot \hat{\mathbf{n}}, \qquad (16)$$

where $\mathbf{U}_{tw}$ is the time-mean thermal wind transport relative to the bottom (explicit use of overbars will be dropped in the following discussion), $\mathbf{u}_{ref}$ is the bottom reference-level velocity, H is the bottom depth, while $\mathbf{U}_{E,s}$ and $\mathbf{U}_{E,b}$ are the top and bottom Ekman transports (the contribution from the surface Ekman layer will be zero if the isopycnal lies too deep). Again, $\hat{\mathbf{n}}$ is the outward-pointing unit vector normal to the contour.

We expect the bottom geostrophic flow to follow the topography in this region, but hydrographic observations will be needed to assess the orientation of the thermal wind currents. A standard gridded product, the $1° \times 1°$ World Ocean Atlas (WOA09: Locarnini *et al.*, 2010; Antonov *et al.*, 2010), actually gives the impression of a significant thermal wind flow straight through the interior regions, especially in the Lofoten and Norwegian Sea basins (Fig. 4, left panel). We are skeptical of this result given the coarse horizontal resolution and given that the product is based on lateral averaging of station data along geopotentials. As argued for and demonstrated by Rossby *et al.* (2009) a more accurate picture of the Nordic Seas hydrography and circulation emerges when the objective mapping is done along neutral or isopycnal surfaces. For this study we, therefore, created a monthly

hydrographic data set for the Nordic Seas at 50–70 km horizontal resolution using isopycnal mapping (Appendix A). This new product shows what we believe is a much more accurate picture of the true hydrographic structure and thermal wind flow (Fig. 4, right panel). In particular, the topographic steering of the scalar fields and hence also of the thermal wind field is striking in comparison to that revealed by WOA09. But closer inspection also reveals some regions where the thermal wind flow does cross the continental slopes, as over the northern flanks of the Voering Plateau near 68°N, 8°E and also farther north near 70°N, 15°E. So it seems the Eulerian mean flow may actually contribute some to the total diapycnal overturning and heat flux convergence, at least in the Lofoten-Norwegian Sea basins.

Reference-level velocities for the geostrophic flow may in principle be estimated directly from surface drifter products or from satellite altimeter estimates of the mean dynamic topography. However, drifters have poor coverage on the western side of the Nordic Seas since they have largely been deployed in the east, and sea ice along the coast of Greenland also causes problems with the altimetric data. So neither drifters nor altimetry can provide very reliable surface velocities for all parts of the Nordic Seas. But another possibility exists. Simplified models of the Nordic Seas have predicted realistic currents when 'forced' with real topography and wind (Nøst and Isachsen, 2003; Isachsen *et al.*, 2003; Aaboe and Nøst, 2008). Built upon the assumption that the bottom geostrophic flow is primarily along isobaths, the models have shown a remarkable agreement with drifter estimates of mean velocities in the eastern Nordic Seas and have also proved to reproduce month-to-month variability and the seasonal cycle well.

For the two closed contours (regions LNb and GSb in Fig. 1) we follow Nøst and Isachsen (2003) and Aaboe and Nøst (2008) and assume that the bottom geostrophic flow is entirely along isobaths. Any geostrophic flow in or out of the two basins is then given by the thermal wind shear relative to the bottom. The thermal wind shear itself is calculated by first interpolating the density onto the topographic contour defining each basin and then estimating horizontal density gradients along that contour.

The thermal wind transport across the contour encircling the larger Nordic Seas interior region (NSi) is estimated similarly as for the two smaller basins. The difference now is that this contour cuts across the Fram Strait at 78°50′N, and there we expect strong cross-contour bottom currents (the flow in and out of the Arctic Ocean). For this stretch our estimate of bottom reference-level velocities will be based on direct observations from a 15-year long current meter mooring array across the Fram Strait (Fahrbach *et al.*, 2001). This array consists of 14 moorings, and all moorings have a current meter placed 10 m above the bottom. We thus use the long-term mean of these lowermost instruments to estimate $\mathbf{u}_{ref}$ (and its uncertainty; see below).

The surface Ekman transport out of a contour is calculated by using surface wind stress from the NCEP-NCAR CDAS-1 climatology according to

$$\mathbf{U}_{E,s} \cdot \hat{\mathbf{n}} = \frac{-(\hat{\mathbf{k}} \times \boldsymbol{\tau})}{\rho_0 f} \cdot \hat{\mathbf{n}}, \tag{17}$$

where $-(\hat{\mathbf{k}} \times \boldsymbol{\tau})$ is the wind stress on the contour rotated clock-wise ninety degrees, ρ_0 is a reference density and f is the Coriolis parameter. The surface Ekman transport is then distributed evenly (linearly) over the upper 50 meters.[5] The bottom Ekman transports are derived from the bottom geostrophic velocities using a linear drag law:

$$\mathbf{U}_{E,b} \cdot \hat{\mathbf{n}} = \frac{R}{f}(\hat{\mathbf{k}} \times \mathbf{u}_{ref}) \cdot \hat{\mathbf{n}} \tag{18}$$

$$= -\frac{R}{f} u^t_{ref} \tag{19}$$

where u^t_{ref} is the (bottom) reference-level velocity tangential to the contour (with shallow water to its right) and $R = 2 \cdot 10^{-4} \mathrm{m\,s^{-1}}$ is a linear drag coefficient (the value chosen has been shown to produce good estimates of large-scale currents in the Nordic Seas and Arctic Ocean by Aaboe and Nøst, 2008). This transport is also distributed uniformly over the lower 50 meters of the water column.

Getting the bottom Ekman flow right thus requires an estimate of the geostrophic bottom flow along the contour. We follow Aaboe and Nøst (2008) and write

$$u^t_{ref} = \left(\frac{g}{\rho_0 f} \rho'_b - \frac{1}{\rho_0 f} \frac{dp_0}{dH} \right) |\nabla H|, \tag{20}$$

where g is the acceleration of gravity, $\rho'_b = \rho_b - \langle \rho_b \rangle$ where ρ_b is the bottom density and $\langle \rho_b \rangle$ is some average bottom density. Finally, $dp_0/dH \cdot |\nabla H|$ is the horizontal pressure gradient at the bottom where p_0 is assumed to be a function of H. This expression says that the bottom geostrophic velocity is given by some average pressure drop across the topography, scaled by the local topographic gradient (as in Nøst and Isachsen, 2003), and by along-slope variations in the bottom density—via the thermal wind shear near the bottom (Walin *et al.*, 2004; Nilsson *et al.*, 2005). So if we know dp_0/dH and bottom densities we are also in a position to estimate the tangential bottom velocity and bottom Ekman transport everywhere on the contour. For the closed Lofoten-Norwegian Sea and Greenland Sea basins we find dp_0/dH by enforcing total top-to-bottom volume conservation within the contour, i.e. by insisting that the bottom Ekman layer balance any divergence in the other transport terms. However, for the NSi contour this method cannot be used since the bottom flow is not tangential to the contour everywhere (the flow through the Fram Strait). Here we instead find the dp_0/dH that gives a bottom velocity equal to the observed bottom flow at 1250 m contour in the Fram Strait.

Top-to-bottom volume is perfectly conserved within the LNb and GSb contours by construction. However, for the NSi contour we cannot expect perfect volume conservation since we are combining an imperfect model with imperfect observations (the flow in the Fram Strait). To enforce *approximate* volume conservation within this contour as well we use

5. Ocean observations of Ekman layer thickness generally fall in the range 25–100 m (see e.g. Davis *et al.*, 1981; Price *et al.*, 1987).

linear inverse techniques to adjust all bottom reference velocities normal to the contour within prescribed uncertainties. This approximate top-to-bottom volume conservation can be expressed as:

$$\oint (\mathbf{U}_{tw} + H\mathbf{u}_{ref} + \mathbf{U}_{E,s} + \mathbf{U}_{E,b}) \cdot \hat{\mathbf{n}}\, ds \lesssim r, \tag{21}$$

or, by the definition $u^n_{ref} = \mathbf{u_{ref}} \cdot \hat{\mathbf{n}}$,

$$\oint H\left(u^n_{ref} + \delta u^n_{ref}\right) ds \lesssim r - \oint (\mathbf{U}_{tw} + \mathbf{U}_{E,s} + \mathbf{U}_{E,b}) \cdot \hat{\mathbf{n}}\, ds, \tag{22}$$

where δu^n_{ref} is a possible correction to the bottom reference velocity and r is a value for the accepted residual in the volume budget. In this budget $\mathbf{U}_{tw}$ is of course the total (bottom-to-top) thermal wind shear, and $\mathbf{U}_{E,s}$ and $\mathbf{U}_{E,b}$ are the two total Ekman transports. Along the 1250 m isobath we now allow nonzero cross-slope bottom geostrophic velocities as long as their kinematic interaction with the topographic slopes does not lead to vertical velocities higher than the average Ekman pumping velocity over the region. Thus, along the 1250 m isobath, we allow corrections within the bound $\delta u^n_{ref} \lesssim W/|H|$ where $W = 2 \cdot 10^{-6}\mathrm{m\,s^{-1}}$ is a reasonable value for the average surface Ekman pumping velocity over the Nordic Seas (see Fig. 2 in Nøst and Isachsen, 2003). Along the part of the contour that follows 78°50′N in the Fram Strait the uncertainties must be estimated by different means. A study of the current meter data from this region shows that the multi-year temporal means are rather stable. The main source of uncertainty is instead tied to the spatial distribution of currents and, specifically, to whether the spatial scales are resolved or aliased by the current meter array. Using the magnitude of spatial variability at the smallest scales as a guide, we judge that that $\delta u^n_{ref} \lesssim 5 \cdot 10^{-3}\mathrm{m\,s^{-1}}$ is a reasonable bound for the correction there.

We now vary u^n_{ref} everywhere along the NSi contour within the prescribed error bounds such that (22) is satisfied with $r = 0.5\,\mathrm{Sv}$ chosen as an acceptable error for the volume budget. Formally, this is a least squares problem where we minimize a weighted sum of the (squared) volume conservation error and the (squared) correction to our initial estimates for reference-level velocities (see e.g. Wunsch, 1996, Chapter 3). Finally, the above error bounds on u^n_{ref} are also used to estimate the uncertainty of the Eulerian mean overturning transport (see below).

d. Eddy-induced transport

The established way to parameterize eddy density fluxes in today's ocean climate models is the GM scheme (Gent and McWilliams, 1990; Gent *et al.*, 1995). For the ocean interior (away from surface and bottom mixed layers) horizontal density fluxes are specified to be adiabatic, down the horizontal density gradient and up the vertical gradient, thus allowing

the release of available potential energy everywhere. The transport streamfunction for the eddy-induced flow (relative to the bottom) takes the form

$$\mathbf{U}^{\#}_{GM} = \frac{\kappa \nabla_h \overline{\sigma}}{\partial_z \overline{\sigma}}, \tag{23}$$

where $\overline{\sigma}$ is the time-mean potential density, ∇_h and ∂_z are the horizontal and vertical gradient operators, and κ is some transfer coefficient or diffusivity for the horizontal potential density flux. To enforce zero eddy-induced flow through the top and bottom boundaries the GM streamfunction must be tapered to constant values there. If one also insists that the parameterization mimic a pure baroclinic overturning with zero depth-integrated flow the streamfunction must take on the same value at the two boundaries. In practice the GM streamfunction is therefore tapered to zero at both surface and bottom boundaries.

A best practice for how to taper of the GM streamfunction near the top and bottom boundaries is still debated. A simplest possible solution (e.g. Griffies, 2004) is to let $\boldsymbol{U}^{\#}$ fall off linearly to zero over the extent of top and bottom mixed layers. As pointed out by Ferrari *et al.* (2008) the problem with this approach is that the eddy-induced velocity will then be discontinuous at the bottom of the surface mixed layer (and at the top of the bottom mixed layer). To circumvent this discontinuity Ferrari *et al.* (2008) proposed a more complicated scheme in which the streamfunction varies linearly through the two mixed layers but then takes on a parabolic shape in additional 'transition layers' between the mixed layers and the ocean interior. Note that in both these schemes the eddy streamfunction falls off linearly within the mixed layers, so the vertical shear of the eddy-induced velocity is zero there and the parameterization will be unable to overturn and re-stratify the mixed layers. Ferrari *et al.* (2008) thus comment that restratification of the mixed layer itself will have to rely on a separate parameterization scheme (see e.g. Boccaletti *et al.*, 2007; Fox-Kemper *et al.*, 2011).

Here we will tackle the complex issue of tapering the GM streamfunction near the top and bottom boundaries by using elements of a recent parameterization proposed by Ferrari *et al.* (2010). The parameterization is given as a boundary value problem for the eddy overturning streamfunction at each horizontal position:

$$\left(c^2 \frac{\mathrm{d}^2}{\mathrm{dz}^2} - N^2\right) \mathbf{U}^{\#} = (g/\rho_0)\kappa \nabla_h \overline{\sigma}, \quad -H < z < 0$$
$$\mathbf{U}^{\#} = 0, \quad z = [-H, 0], \tag{24}$$

where $N^2 = -g/\rho_0 \, \partial_z \overline{\sigma}$ is the squared buoyancy frequency, κ is a diffusivity and c some parameter (taking on the units of speed) which acts to weight the first l.h.s. operator on $\mathbf{U}^{\#}$ relative to the second. The parameterization is in fact a combination of the classic GM scheme (recovered if $c^2 = 0$) and another novel scheme proposed by Aiki *et al.* (2004) (recovered if $N^2 = 0$). Ferrari *et al.* (2010) focused specifically on eddy stirring by the

barotropic mode and hence argued for depth-independent c^2 and κ. In this study we will instead use (24) as a *general form of the GM streamfunction* by prescribing $c^2 = 0$ in the ocean interior, effectively insisting that the eddy transport be adiabatic and release available potential energy there. Then by introducing a nonzero c^2 in top and bottom mixed layers we will use the second-order differential operator to ensure the required tapering to zero at the boundaries. One may possibly think of c^2 as being related to the kinetic energy level of the three-dimensional small-scale turbulence responsible for diabatic mixing. This fits the phenomenology of low diabatic mixing rates in the ocean interior and high mixing rates near the top and bottom boundaries. But for now, lacking any observational or theoretical evidence for such a possible relationship, we will simply let c^2 grow linearly—from zero at the mixed layer base to some finite value c_0^2 at the top (or bottom) boundary.[6] Assuming that the eddy overturning is related to deep Eady-type instability and that a steady state exists in which there is a balance between diabatic mixing and adiabatic restratification of the surface and bottom mixed layers, we will set c_0 equal to the phase speed of the first baroclinic mode (as did Ferrari *et al.*, 2010).

The second free parameter to be specified is the eddy diffusivity κ. This is a research topic in its own right, and here too there is little consensus on a best general form. For this study we will try three different choices for the horizontal structure of diffusivities, starting with the simplest possible option, a constant diffusivity:

$$\kappa_c = 1000\,\mathrm{m^2\,s^{-1}}.$$

We also test the classical scaling proposed by Stone (1972), that is a diffusivity scaled by the parameters relevant for the Eady problem, i.e. the top-to-bottom thermal wind shear V_{tw} and the first baroclinic deformation radius L_d:

$$\kappa_S = \alpha_S V_{tw} L_d,$$

with α_S being some efficiency coefficient. Note that if one replaces the deformation radius with the width of a baroclinic front as the relevant mixing length this expression becomes equivalent to one proposed by Spall and Chapman (1998) and later used in idealized studies by Straneo (2006b) and Spall (2004, 2005, 2010a,b). For our study we chose to use the Stone (1972) form since the width of a front is notoriously difficult to define, except for in very idealized 2D geometries. In the calculations to be presented below the thermal wind shear and the internal deformation radius were calculated, month-to-month, from the new hydrographic climatology. Finally, to allow for the possibility of nonlocal sources of eddy

6. Setting c^2 to a constant in the top and bottom mixed layers would even simpler, but this would introduce discontinuities into the equation. If c^2 is indeed tied to the kinetic energy of boundary-generated small-scale turbulence, then one expects a gradual leveling off towards the ocean interior.

kinetic energy, we also test diffusivities based on measurements of sea surface variability, as proposed by Holloway (1986):

$$\kappa_H = \alpha_H \frac{g}{|f|} (\overline{\eta'^2})^{1/2}. \tag{25}$$

Here $\overline{\eta'^2}$ is the SSH temporal variance, g is the acceleration of gravity, f the Coriolis parameter and α_H is another efficiency coefficient. This is not a parameterization *per se* since it requires information of the eddy field itself, but it is a diagnostic relationship[7] which has proved useful for studies of eddy transport in the Southern Ocean (Keffer and Holloway, 1988; Karsten and Marshall, 2002).

Constructing reliable Holloway diffusivities at high latitudes is somewhat problematic. In this study we will be using the Ssalto/Duacs gridded Sea Level Anomaly (SLA) fields produced by AVISO which come at 7-day intervals on a $1/3°$ Mercator grid (AVISO, 2011). At the latitudes of the Nordic Seas the AVISO gridded product uses data from the ERS and Envisat satellites which are polar orbiting and from the GFO satellite which reaches 72°N. The repeat cycles are 35 days for ERS and Envisat and 17 days for GFO, but, partially compensating for the low time resolution, both types of orbits have relatively small track spacing at these high latitudes (about 20 km at 75°N for either ascending or descending orbits of Envisat). The product should thus be able to give some useful information of SLA variance if integrated over spatial scales over a few tens of kilometers. The smallest eddies will be under-sampled, but if lateral mixing is primarily done by the largest eddies the error may not be too serious.[8] However, the along-track data that goes into the gridded products is also heavily smoothed, so one cannot but anticipate that the final gridded product underestimates the true SLA variability somewhat. To get an idea of the quality of the SLA product we therefore did a comparison between eddy kinetic energy (EKE) levels obtained from the SLA products (by calculating the SLA gradient) and from surface drifters (Andersson *et al.*, 2010; Koszalka *et al.*, 2011). The results (not shown here) indicated that SLA EKE is about a factor four to five lower than drifter EKE, but that the spatial patterns are in good agreement.

In Appendix B we study near-surface eddy buoyancy transport in primitive equation simulations of an idealized channel with and without a sloping bottom. The idealized simulations indicate that all three forms of diffusivities (with $\alpha_S \sim 25$ and $\alpha_H \sim 0.8$ for the Stone and Holloway forms, respectively) give reasonable parameterized eddy transport if the bottom is flat. But the simulations also show that the down-gradient parameterization, particularly when using Stone diffusivities κ_S, is overestimating the real transport when a bottom slope is introduced. As argued by Blumsack and Gierasch (1972) and Mechoso (1980), and recently verified with idealized numerical simulations by Isachsen (2011), the

7. The expression is based on the assumption that the effective diffusivity caused by quasi-geostrophic eddy stirring scales with the velocity amplitude and wavelength of each Fourier component. A total diffusivity is then formed by taking an integral under the wavenumber spectrum. (Holloway and Kristmannsson, 1984).

8. For a red kinetic energy spectrum the error formally depends on the steepness of the spectrum, as discussed by Bennett (1984).

potential vorticity gradient of the slope affects both growth rates and length scales of unstable Eady waves, typically reducing the magnitude of both.

Suppression of diffusivities over a sloping bottom may also be related to a purely kinematic effect of the mean jet that typically forms there, as recently proposed by Ferrari and Nikurashin (2010). The argument is that growing waves in a baroclinically unstable jet typically propagate against the mean current, and the mean flow advection of a tracer in that jet will lower the correlations between velocity and tracer perturbations that set the strength of the cross-jet mixing. They proposed an effective diffusivity that goes like

$$\kappa_{eff} = \frac{\kappa}{1 + d_2 V_0^2 / EKE}, \tag{26}$$

where κ is the diffusivity in the absence of mean flow, V_0 is the mean current speed and *EKE* is eddy kinetic energy. The parameter d_2 reflects both the proportionality between eddy interaction time and eddy strain rate and the proportionality between eddy phase speed and mean current speed. Ferrari and Nikurashin found that $d_2 = 4$ gave the best comparison with independent calculations of diffusivities in the Antarctic Circumpolar Current, while Eden (2011) argued for $d_2 = 1$ based on an analysis of idealized numerical simulations. For our idealized channel simulations in Appendix B we found that invoking Ferrari–Nikurashin suppression with $d_2 = 2$ improved the comparison with diagnosed diffusivities and cross-channel transport considerably.

Figure 5 shows our estimates of annual-mean eddy diffusivities over the Nordic Seas from the Stone (1972) parameterization (with $\alpha_S = 10$) and from the Holloway (1986) diagnostic expression ($\alpha_H = 0.8$). Holloway diffusivities are based on SLA variability on sub-monthly time scales from the period Jan. 2001 to Dec. 2010 (roughly the overlap period of the Envisat and GFO altimeter instruments). In both cases the kinematic suppression suggested by Ferrari and Nikurashin (2010) has been applied (the mean flow strength V_0 was estimated from thermal wind and *EKE* from altimetry, scaled by a factor of four). Mean jet suppression is most clearly seen in the Holloway diffusivities along the Atlantic Water path in the east and along the JMK Ridge. In general, the Holloway estimate here is in good agreement with drifter estimates recently published by Koszalka *et al.* (2011; see e.g. their Figs. 6 and 9), although its magnitude is roughly a factor two lower[9]. Both estimates suggest that diffusivities are enhanced east of the JMK Ridge and that the very highest diffusivities are found in the Lofoten basin. As pointed out by Köhl (2007) the high eddy activity there partially reflects the presence of a quasi-permanent anticyclone, formed by the merging of anticyclones originating from the continental slope along northern Norway. Even if they are not locally generated, the anticyclones likely have the net effect of enhancing lateral stirring in the region.

9. We expect altimeter EKE to be more severely affected by the smoothing that goes into the gridded products. The geostrophic sea level velocities go like $u' = -g/f\,\partial_x \eta'$, so the EKE spectrum goes like $(g/f)^2 k^2 \tilde{\eta}'^2$ for SLA Fourier component $\tilde{\eta}'$ at wavenumber k. The high wavenumbers that are most damped by the smoothing are thus preferentially weighted in the EKE spectrum (compared to a spectrum of diffusivities that goes like $(g/f)^2 \tilde{\eta}'^2$).

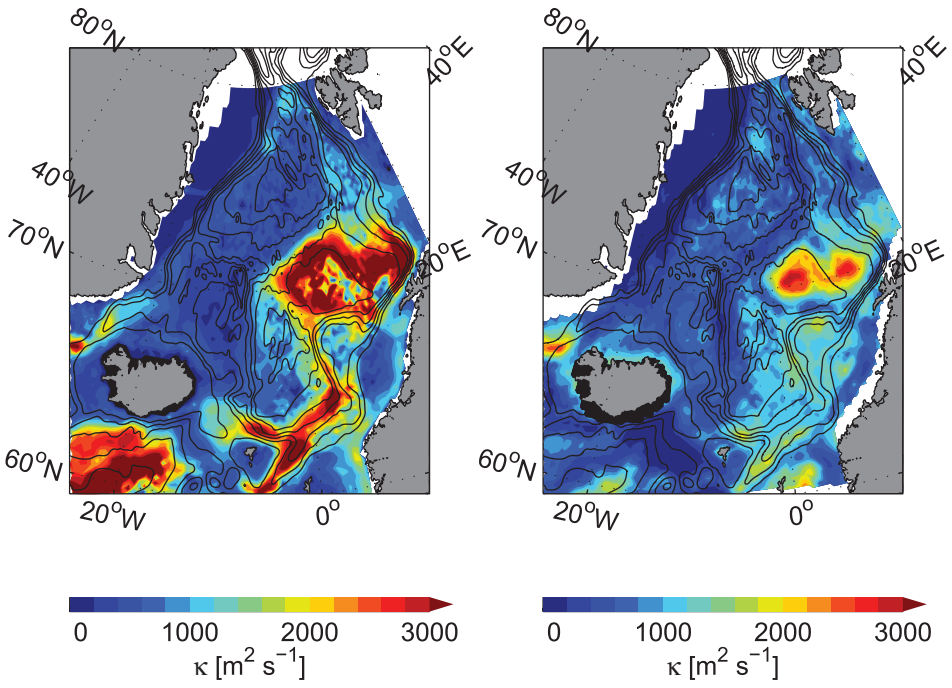

Figure 5. Estimates of annual-mean surface eddy diffusivity based on (left) the Stone (1972) parameterization involving the top-to-bottom thermal wind shear and the first internal deformation radius, and (right) the diagnostic expression of Holloway (1986) involving the sea surface height variability. The kinematic suppression suggested by Ferrari and Nikurashin (2010) has been applied to both fields.

Since the Stone (1972) parameterization does not account for nonlocal sources of eddy kinetic energy, it fails to capture the enhanced eddy activity in the central Lofoten basin. Instead, the Stone estimate predicts the highest diffusivities over the topographically-locked frontal regions. But, as discussed above (and seen in Appendix B), we are suspicious of the suggested enhancement there, since the parameterization is unable to account for a possible topographic suppression of baroclinic instability. Indeed, the Stone diffusivities in Figure 5 had to be scaled down by a factor two and a half ($\alpha_S = 10$) from those found to fit in the simulations of Appendix B to keep the magnitude within a reasonable range over the sloping topography.

Despite these problems, the Stone estimate shares important similarities with the altimetry estimate, notably by indicating that diffusivities are higher in the eastern parts of the domain—the region with the highest baroclinicity. And, in truth, there is very little prior knowledge of what actual eddy diffusivities *should* look like in this region. The Holloway diffusivities appear to be best in agreement with the recent drifter estimates of Koszalka *et al.* (2011), but they too are problematic (being biased low, as we've seen). Therefore, below

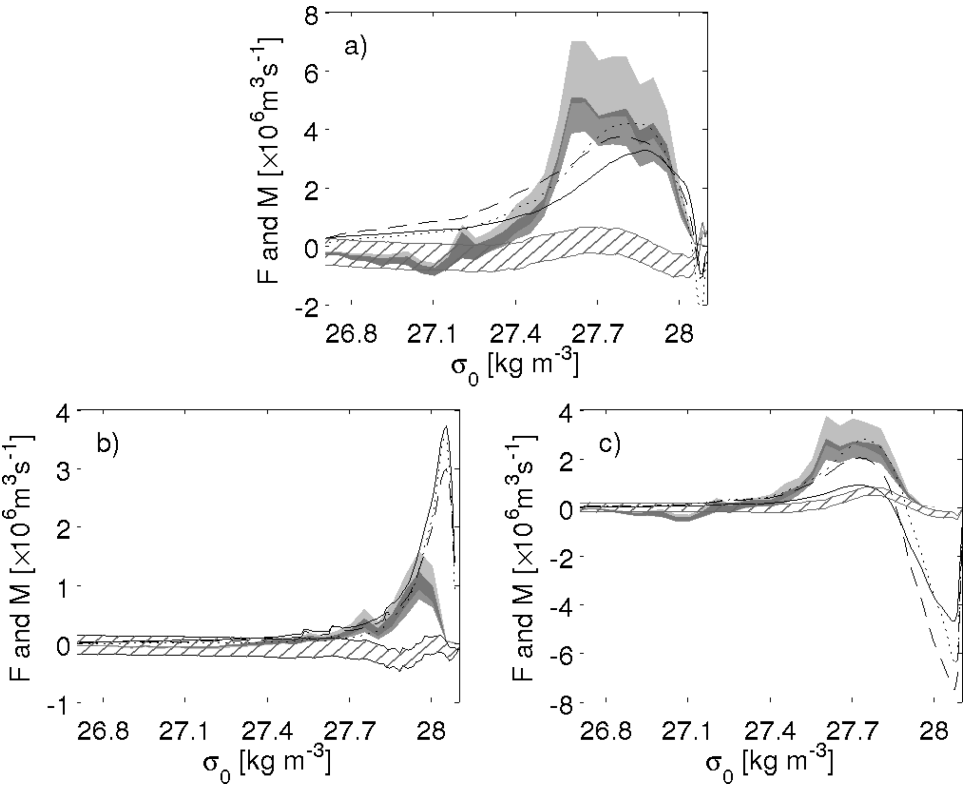

Figure 6. Estimates of the annual-mean air-sea density transformation and diapycnal overturning circulation for (top) the Nordic Seas interior box, (lower left) the Greenland Sea box and (lower right) the Lofoten-Norwegian Sea box. The air-sea transformation $\langle \hat{F} \rangle$ is shown with gray shading (as in Fig. 3), the mean-flow overturning $\langle \overline{M} \rangle$ is shown as a hatched region while the eddy-induced overturning $\langle M^{\#} \rangle$ is shown as lines, estimated with three different horizontal eddy diffusivities: (solid) constant diffusivity, (dashed) Stone diffusivity and (dotted) Holloway diffusivity.

we will present estimates of the eddy overturning in this region using all three (including constant) estimates of the eddy diffusivities.

3. Results

a. Estimates of the air-sea transformation and diapycnal overturning

Figure 6 shows our estimates of the annual-mean air-sea density transformation $\langle \hat{F} \rangle$ and the diapycnal overturning circulation (mean contribution, $\langle \overline{M} \rangle$, and eddy contribution $\langle M^{\#} \rangle$) for the three interior regions of the Nordic Seas. The sign conventions are as in Figure 3: positive $\langle \hat{F} \rangle$ indicates creation of denser watermasses by air-sea fluxes, and a positive slope $\partial \langle \hat{F} \rangle / \partial \sigma > 0$ requires—if turbulent diapycnal fluxes are small—a net inflow. Similarly, a

positive slope for $\langle \overline{M} \rangle$ or $\langle M^{\#} \rangle$ indicates a net import of waters by the mean or eddy-induced flow, respectively.

It is clear that advection by the mean flow is unable to balance the annual-mean surface transformation. For the Nordic Seas interior box (NSi) the primary mean-flow overturning cell consists of import of water with potential density in the range $27.2 < \sigma_0 < 27.7\,\mathrm{kg\,m^{-3}}$ and export of waters denser than this. It has a magnitude of about 1 Sv compared to an air-sea transformation of 4–6 Sv for the same density range. There is also some indication of an import of very dense waters ($\sigma_0 > 28\,\mathrm{kg\,m^{-3}}$) which can only come from the Arctic. But, considering the uncertainties in our estimate of the bottom flow in the Fram Strait, this may not be a very robust result. What stands out in this calculation is that the bulk of the transformation between $27.2 < \sigma_0 < 28\,\mathrm{kg\,m^{-3}}$ must be balanced by eddy-induced advection. And, as it turns out, the parameterization used here is able to trace out the gross features of the transformation curve for all three choices of eddy diffusivity. The values of the scaling parameters used are as in the previous section, except that Holloway diffusivities have been multiplied by an additional factor two to make them more in line with the drifter diffusivities of Koszalka *et al.*, 2011 (see the discussion about magnitudes in Section 2d). Compared to the air-sea transformation, the parameterization appears to exaggerate the import of the very lightest density classes ($\sigma_0 < 27.4\,\mathrm{kg\,m^{-3}}$) at the expense of denser classes. But when the modest contribution from the mean-flow advection is added, there is quite a good fit between the total overturning and the surface transformation.

The corresponding estimates for the two smaller sub-basins generally confirm the same story. In the stratified Lofoten and Norwegian Sea basins the mean flow seems to contribute some, perhaps as much as 25%, to the total overturning. Here the mean flow transport is dominated (not shown) by the thermal wind component which, as we have seen in Figure 4, is able to rotate and cross the topography in some places. In the Greenland Sea, however, the thermal wind transport is negligible due to the weak stratification, and the only contribution comes from Ekman current. But the predominance of cyclonic winds over the Greenland Sea sets up mean Ekman currents that import dense waters and export light waters, so the mean flow therefore appears to contribute with the opposite sign as would be required to balance the air-sea transformation. Again, eddy-induced advection must be responsible for the bulk of the density transport in and out of these regions.

But, as it turns out, the predictions by the eddy parameterization are here less consistent with air-sea fluxes. While nicely predicting the import of light waters into both basins, the parameterization appears to wildly overestimate the overturning at high densities. It suggests a very strong intermediate-to-dense ($27.9 < \sigma < 28.1\,\mathrm{kg\,m^{-3}}$) overturning in the Greenland Sea basin and an almost perfectly corresponding dense-to-intermediate overturning in the Lofoten–Norwegian basins. This suggests that intermediate waters are transported westward across the Jan Mayen-Mohn-Knipovitch Ridge and that denser waters are returned eastward, with a total overturning strength in the range 3–8 Sv. There is every reason to be skeptical of this result. The air-sea flux data do confirm that there is an intermediate-to-dense transformation at the surface in the Greenland Sea, but the magnitude here is no

more than 2 Sv. And, more importantly, in the Lofoten-Norwegian Sea basins there is no trace whatsoever of an air-sea transformation back from dense to intermediate waters.

The parameterization must be getting something wrong, and the most obvious candidate is the depth-independent diffusivities that have been used. If diffusivities instead decay with depth the overturning strength at depth would presumably decrease. As it turns out, several recent studies have pointed to the need for depth-dependent eddy diffusivities in order to make ocean circulation models consistent with the observed hydrographic structure (Danabasoglu and Marshall, 2007; Eden *et al.*, 2009). Diagnostics studies of diffusivities themselves have also indicated depth-dependence and, more specifically, surface-intensification of diffusivities (Ferreira *et al.*, 2005; Olbers and Visbeck, 2005; Le Sommer *et al.*, 2011).

Depth-dependent diffusivities are readily possible in the linear instability problem (Green, 1970; Killworth, 1997; Eden, 2011) and it seems that enhanced diffusivities high in the water column may be related to the presence of steering or critical layers there (Smith and Marshall, 2009; Abernathey *et al.*, 2010). But no simplified scaling solutions for use in parameterizations have yet been proposed. In this study we will not pursue theory in more detail, but we will nonetheless try out two very idealized depth-dependent forms. The idea is to see whether the parameterized eddy fluxes can be brought into better qualitative agreement with the observed air-sea fluxes. Specifically, we will keep using the Holloway form (25) for the horizontal structure and will also assume that diffusivities are constant within the surface mixed layer. But below the surface layer the diffusivities will decay with depth using two different structural forms. The depth of the surface mixed layer will be determined as in Large *et al.* (1997) and Fox-Kemper *et al.* (2011) as "the shallowest depth where the local, interpolated buoyancy gradient matches the maximum buoyancy gradient between the surface and any discrete depth within that water column." Then, in the first of the two formulations the diffusivity below the mixed layer is specified as

$$\kappa = \frac{\kappa_{ml}}{\sqrt{1 + \left(N_{ref}^2 / N^2\right)^2}}, \tag{27}$$

where κ_{ml} is the mixed layer diffusivity (given by Eq. 25) and N_{ref} is the maximum buoyancy frequency at the mixed layer base (as defined above). This formulation ensures a smooth transition between the constant value in the mixed layer and an N^2-dependence at depth as observed in an adjoint model by Ferreira *et al.* (2005; see their Fig. 13). In a second formulation the diffusivity below the mixed layer is simply set to decay exponentially as

$$\kappa = \kappa_{ml} e^{(z - z_{ml})/h_e}, \tag{28}$$

where z_{ml} is the level of the mixed layer base and h_e is some decay depth which we think of as the decay depth for EKE (assuming mixing time scales are depth-independent). Drawing on the diagnostics of EKE penetration depths in eddy-permitting models by Yim *et al.* (2010) and Venaille *et al.* (2011), we present results below based on $h_e = 150\,\mathrm{m}$.

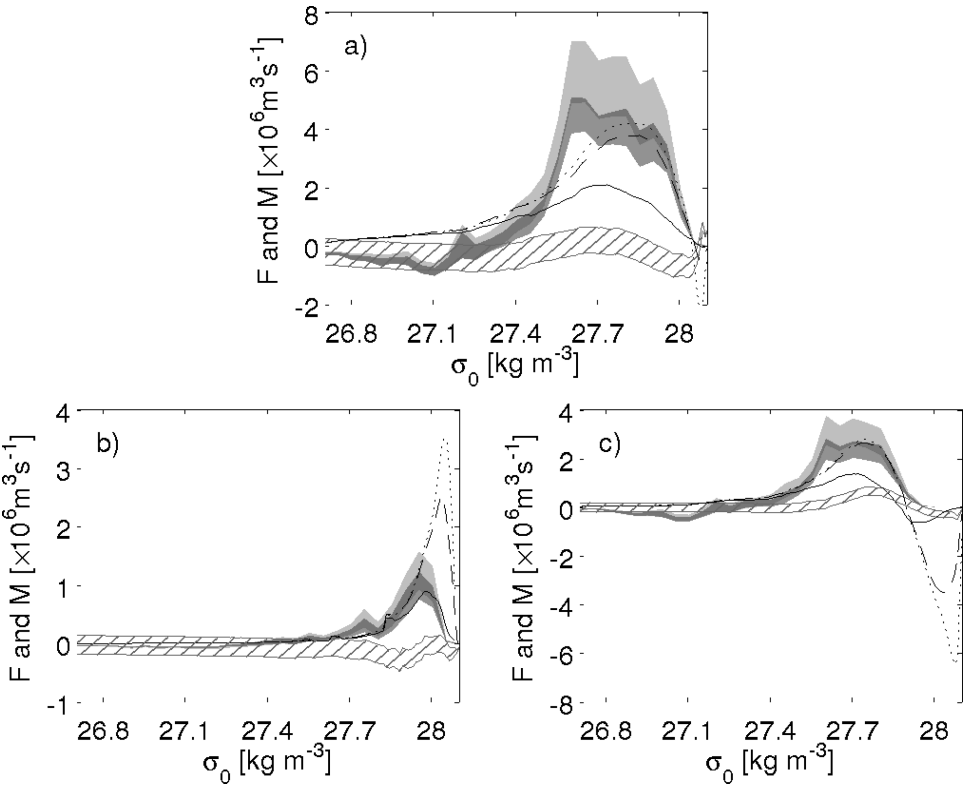

Figure 7. Same as in Figure 6 but now only for Holloway diffusivities that have been assigned three different vertical structures: (dotted) constant, (dashed) N^2-dependence, and (solid) exponentially-decaying dependence.

The overturning rates resulting from these new calculations are shown in Figure 7 (along with the earlier result using depth-independent diffusivities). As expected, the proposed eddy-induced overturning at higher densities is reduced in all three regions. Judging by the comparison with the air-sea transformation, it appears that the N^2-dependent form underestimates the suppression at depth while the exponentially-decaying form overestimates it somewhat. But, given the ad hoc form of the diffusivities, a close quantitative agreement with the air-sea flux data should of course not be expected. We simply take the results of this exercise as indication that diffusivities are most likely surface-intensified, as has been suggested for other regions of the world ocean. The estimated deep overturning between the east and west can now be reduced to 0.5–1 Sv (for the exponentially-decaying form), a magnitude which is at least plausible, as we will see in the discussion below.

Figure 8 shows the annual-mean potential density field and the parameterized annual-mean eddy-driven overturning streamfunction (with exponentially decaying diffusivities

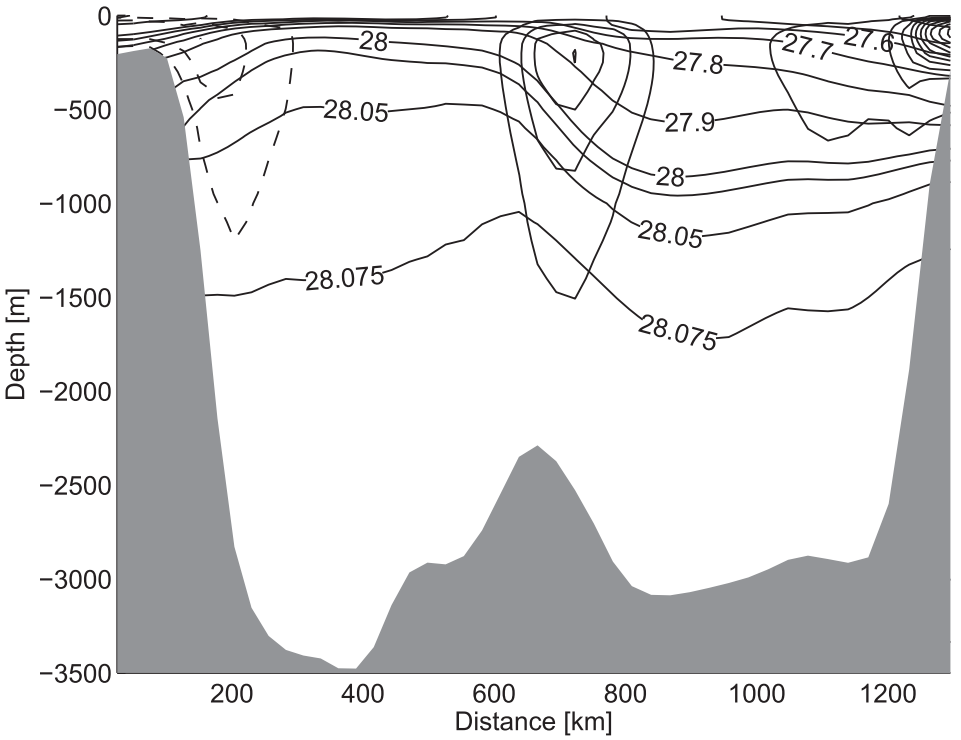

Figure 8. Annual-mean (black contours) potential density σ_0 and (gray contours) eddy-induced streamfunction (Holloway diffusivities with exponentially-decaying depth dependence) for a transect crossing the Nordic Seas from the north-west to the south-east (see Fig. 1). The contour interval for the streamfunction is $0.25\,\mathrm{m^2 s^{-1}}$ and dashed lines indicate negative values.

below the surface mixed layer) for a transect that crosses the Nordic Seas from the north-west to the southeast (as traced out in Fig. 1). The circulation cells in this figure should not be taken as representing advection paths of individual water parcels, but to the extent that the parameterization works they can be taken as indication of exchanges in an integrated sense. The parameterization suggests a relatively modest clockwise overturning between the buoyant East Greenland Current residing over the continental slope east of Greenland and the dense waters of the deep Greenland Sea, and it also suggests a much stronger counter-clockwise overturning between the Norwegian Atlantic current flowing along the Norwegian coast and the deep Lofoten basin. Both circulation cells are consistent with the presence of baroclinic fronts (presumably unstable) between the boundary currents and the interior basins, and they also fit our prior understanding of the exchanges that actually take place.

Equally noticeable is the suggested counter-clockwise overturning cell between the Lofoten and Greenland Sea basins. This cell is weaker than the cell off the Norwegian

coast, but it is deep and implies the export of waters denser than $\sigma_0 \simeq 27.9\,\mathrm{kg\,m^{-3}}$ from the west, subsurface diapycnal 'upwelling'[10] in the east and transport of the lighter (intermediate density) waters to the west again. That there should be baroclinic instability and eddy transport between the eastern and western basins is to be expected from the strong baroclinicity seen above the JMK Ridge. The idealized numerical simulations of Spall (2010b) have demonstrated that this process is likely at play, and it is also worth noting that a recent diagnostic study by Segtnan *et al.* (2011) concludes that eddy-induced transport must take place across the JMK ridge system for heat and freshwater budgets in both the east and west to balance. But, as discussed above, we find no observational evidence of a dense-to-light transformation of the very highest density classes by air-sea fluxes in the east. The eastern basins also experience a net buoyancy loss to the atmosphere over the year, and during summer, when there is a modest warming, the densest water masses in question do not outcrop.

One possible explanation for the missing balance in the Walin budget is that the eddy-driven exchanges across the JMK Ridge are tied to other lateral exchanges in the Lofoten-Norwegian Sea basins that we have either quantified incorrectly or failed to capture entirely. Specifically, the dense waters entering into the eastern basins by eddies may conceivably be exported out by some time-mean currents undetected by our datasets or simplified model. Or, as suggested to us by one of the reviewers, this dense water may actually be exported into the main boundary current by an eastern eddy-driven overturning cell (see Fig. 8) which in reality is stronger and deeper than our parameterization suggests.

The possibility of undetected mean currents and links between the central and eastern eddy-driven overturning cells both warrant further study. But below we will look into an entirely different and hitherto neglected process that may also close the Walin budget in these sub-basins: turbulent diapycnal mixing. Is the suggested eddy-driven overturning cell across the Jan Mayen-Mohn-Knipovich Ridge in fact sustained by a subsurface, mixing-driven, dense-to-light transformation in the east?

b. Estimates of turbulent diapycnal density fluxes

In summary, the results so far have indicated that our estimates of the residual diapycnal overturning circulation through interior regions of the Nordic Seas agree, by and large, with the observed air-sea density transformation—but only if eddy-induced transport is included. There are, however, also notable discrepancies, most strikingly exemplified by the last suggestion of an eddy-induced 0.5–1 Sv overturning flow between the east and the west for $\sigma_0 \gtrsim 27.8\,\mathrm{kg\,m^{-3}}$ that has absolutely no corresponding signature in the air-sea fluxes. And, at the other end of the density scale, the Walin calculation suggests a net production of very light waters ($\sigma_0 \lesssim 27.2\,\mathrm{kg\,m^{-3}}$) by air-sea fluxes in the Nordic Seas

10. Strictly speaking, the term 'upwelling' refers to the *vertical* movement of water rather than the diapycnal flow from dense to light (Spall and Pickart, 2001). But when discussing the movement of water properties, as we do here, the total (residual) upwelling may have an eddy-induced component.

interior box (NSi) that does not appear to be balanced by advection. The magnitude of this transformation, about 0.5 Sv, is arguably within the error bounds of our calculations, but it is a consistent feature in the flux climatologies and likely reflects actual surface warming during summer. There is only a very slight, if any, indication of a diapycnal overturning at these densities for the Nordic Seas interior box (Fig. 6). Could turbulent diapycnal density fluxes be responsible for either or both of these discrepancies?

Previous studies have generally found turbulent fluxes to be of second-order importance to high-latitude budgets, but to neglect them completely, as we have done so far, may also be an extreme over-simplification. Such diapycnal fluxes can schematically (e.g. Nurser *et al.*, 1999) be divided into three categories: quasi-horizontal fluxes driven by mesoscale or submesoscale eddies in the surface mixed layer (denoted as D_{horiz}), fluxes through the base of the surface-mixed layer during intense mixing events (D_{mlb}), and quasi-vertical fluxes driven by small-scale background mixing in the deep ocean (D_{vert}). The convergence of diapycnal turbulent density fluxes may thus be written:

$$-\frac{\partial D}{\partial \sigma} = -\frac{\partial}{\partial \sigma}(D_{horiz} + D_{mlb} + D_{vert}). \tag{29}$$

Below we will estimate a possible contribution from eddy mixing in the surface mixed layer and also make a very rough assessment of the impact from vertical mixing at depth.

The net effects of lateral eddy stirring near the surface was studied in eddy-resolving numerical calculations by Cerovečki and Marshall (2008). They found that diabatic eddy fluxes in the surface layers generally oppose the tendency of air-sea fluxes. For our present purpose near-surface diapycnal eddy fluxes will be estimated as in Nurser *et al.* (1999) by assuming horizontal down-gradient eddy fluxes over the depth of the mixed layer and integrating over the length of the outcrop positions of a given potential density:

$$D_{horiz} = \int -\kappa_{ml} |\nabla \overline{\sigma}_{ml}| h_{ml} \, ds, \tag{30}$$

where κ_{ml} is the near-surface horizontal eddy diffusivities (here, again, estimated from the sea surface height variability), $\nabla \overline{\sigma}_{ml}$ is the horizontal gradient of depth-averaged mixed layer potential density and h_{ml} is the depth of the mixed layer. The resulting estimate for the Nordic Seas interior (NSi) box is shown in Figure 9. The calculation by and large agrees with the conclusions of Cerovečki and Marshall (2008) in suggesting that eddy mixing tends to erode the formation of light water masses made by air-sea fluxes during summer and also opposes some of the formation of dense waters made by air-sea fluxes during winter.

An estimate of turbulent vertical mixing at depth will necessarily be much cruder given the difficulty of observing mixing intensity in the deep ocean. Here we will limit ourselves to a lowest-order estimate of mixing in the Lofoten-Norwegian Sea basins based on observed

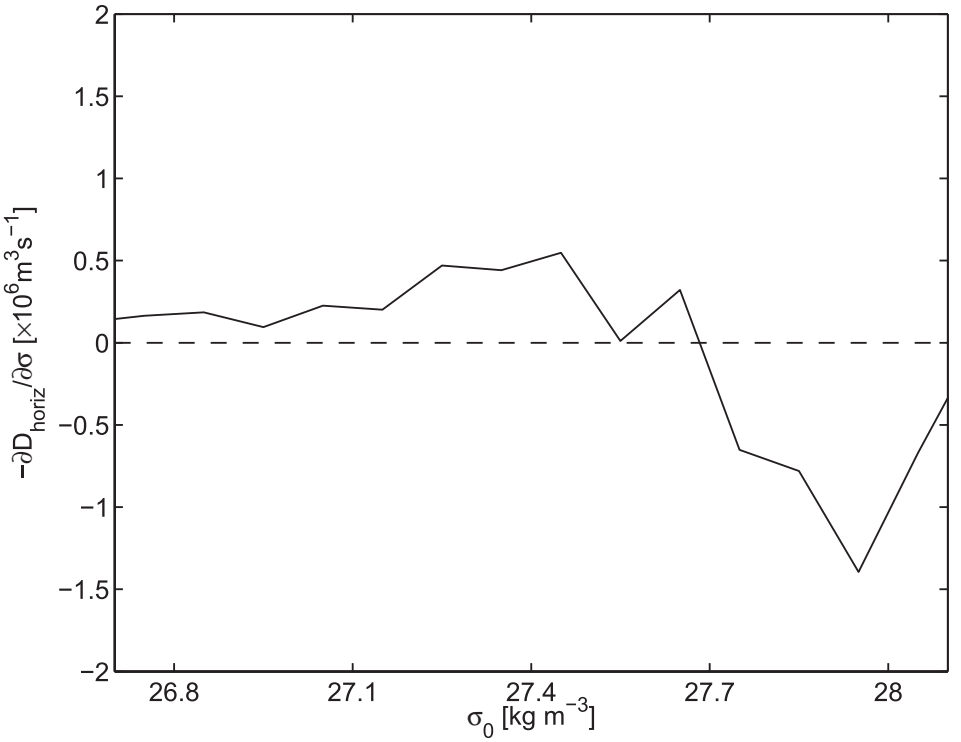

Figure 9. Estimate of the annual-mean convergence of diapycnal density fluxes in the mixed layer by eddies, $-\partial D_{horiz}/\partial\sigma$, for the Nordic Seas interior (NSi) box.

turbulent dissipation rates presented by Naveira Garabato *et al.* (2004). If we assume, as they did, that a vertical (diapycnal) diffusivity scales as

$$K = \Gamma\epsilon/N^2, \tag{31}$$

where ϵ is the dissipation rate and $\Gamma \sim 0.2$ is the mixing efficiency (Osborn, 1980), then the vertical turbulent density flux will be

$$\begin{aligned}\overline{w'\sigma'} &= -K\frac{\partial\sigma}{\partial z}\\ &= \Gamma\epsilon\frac{\rho_0}{g}.\end{aligned} \tag{32}$$

Note that in the Walin framework (see Fig. 2) this means that $D_{vert} < 0$, i.e. a density flux from high to low densities. The convergence of this flux, integrated over a given isopycnal, is therefore

$$-\frac{\partial D_{vert}}{\partial\sigma} = -\frac{\partial}{\partial\sigma}\iint\left(-\Gamma\epsilon\frac{\rho_0}{g}\right)dA. \tag{33}$$

Naveira Garabato *et al.* (2004) presented profiles of ϵ for the Greenland Sea and the Norwegian Sea (their Fig. 3). Neglecting the change in isopycnal area with depth, an estimate can thus be made from

$$-\frac{\partial D_{vert}}{\partial \sigma} \simeq \Gamma \frac{\rho_0}{g} A \frac{\partial \epsilon}{\partial \sigma} \simeq -\Gamma A \frac{\partial \epsilon}{\partial z} N^{-2}. \tag{34}$$

Their data indicate that mixing intensity in the Norwegian Sea increases with shallower depth in the depth range 1500 m to 700 m. This means *divergent* turbulent density fluxes on isopycnals in this depth range and a dense-to-light diapycnal 'upwelling' of waters which, according to our eddy parameterization, may have entered from the west (Fig. 8). Using their reported dissipation rates $\epsilon \sim 1 \cdot 10^{-10}\mathrm{m}^2\mathrm{s}^{-3}$ and $\epsilon \sim 5 \cdot 10^{-10}\mathrm{m}^2\mathrm{s}^{-3}$ at 1500 m and 700 m, respectively, a mean squared buoyancy frequency $N^2 \sim 1 \cdot 10^{-6}\,\mathrm{s}^{-2}$, a surface area of the Lofoten-Norwegian Sea basin $A \sim 4.5 \cdot 10^{11}\,\mathrm{m}^2$, a mixing efficiency $\Gamma \sim 0.2$, and allowing for their factor three estimate for uncertainty in ϵ we arrive at a dense-to-light diapycnal flow of 0–0.2 Sv. Even the upper bound of this estimate is quite a bit smaller than our most moderate estimate of eddy-induced dense-to-light diapycnal overturning within the Lofoten-Norwegian Sea basin (Fig. 7), so we would be hard pressed to argue that the two estimates are consistent other than in their sign.

The dissipation estimates presented by Naveira Garabato *et al.* (2004) were based on measurements made during late summer and the calculations are based on the assumption that diapycnal mixing is caused by the background internal wave field. As the above rough estimates suggest, this process does not seem capable of sustaining a dense-to-light conversion of the magnitude suggested by the eddy parameterization. However, we can safely assume that upper-ocean mixing rates are much higher during winter months, both due to enhanced wind-driven turbulence and, particularly, due to cooling-driven convection. A method for estimating the density transformation at the base of the mixed layer during strong mixed layer deepening events has been developed by Garrett and Tandon (1997) and later evaluated in several studies (e.g. Nurser *et al.*, 1999; Marshall *et al.*, 1999). Notably, Tandon and Zhao (2004) evaluated this effect in the North Atlantic using reanalysis atmospheric forcing and a set of one-dimensional mixed layer models. They found a contribution of about 0.5 Sv in the overflow region just south of the Greenland–Scotland Ridge, a region with comparable surface area to the eastern parts of the Nordic Seas investigated here. It is at least plausible that the situation in the Nordic Seas is comparable. Note also, as pointed out to us by one reviewer, that intense mixing during winter-time convection may also be responsible for removing some of these very lightest waters created by air-sea fluxes in summer. But making detailed calculations of episodic entrainment during mixed-layer deepening events is beyond the scope of the present study, and we have to conclude that these issues, especially the magnitude of the subsurface overturning circulation across the JMK Ridge, remain unanswered.

4. Summary and discussion

Observations and simplified theory have been used to study the relationship between the air-sea density transformation and the residual diapycnal overturning circulation in interior regions of the Nordic Seas. The mean-flow overturning, consisting of time-mean Ekman and geostrophic currents, appears to make a modest contribution (possibly up to 25%) to the buoyancy transport and overturning in the Lofoten and Norwegian Sea basins east of the Jan Mayen-Mohn-Knipovich Ridge. But in general mean-flow exchanges are severely restricted due to the topographic constraints, and eddy-induced transport must dominate. We have seen that observed air-sea transformation rates can be reasonably well balanced if eddy density transport is parametrized with a modified GM scheme that also incorporates top and bottom boundary layers.

Systematic discrepancies between our estimates of the air–sea transformation and the advective overturning have also been found. The air-sea flux data suggests a net formation during summer of very light water masses ($\sigma_0 \lesssim 27.2\,\mathrm{kg\,m^{-3}}$) that seem to be exported from the region neither by the mean flow nor the eddy-induced overturning. However, estimates of quasi-lateral eddy fluxes in the surface mixed layer indicate that this signal from air-sea fluxes may be partially eroded by diapycnal mixing. A more notable discrepancy found is the prediction by the eddy parameterization of a sizable (0.5–1 Sv by our most conservative estimate) export of very dense waters from the west to the east across the JMK Ridge—waters that do not however appear to be made lighter in the eastern basins by air-sea fluxes. Unless these dense waters are exported out of the Nordic Seas by mean currents undetected in our analysis, or by stronger and deeper eddy advection in the east, they must be made lighter in the east by subsurface turbulent mixing. Using observations of turbulent kinetic energy dissipation reported by Naveira Garabato *et al.* (2004), we made very rough estimates of possible dense-to-light conversion rates due to breaking internal waves in the eastern basins. These calculations indicate diapycnal 'upwelling' rates in the range 0–0.2 Sv, i.e. almost an order of magnitude smaller than those suggested by the eddy parameterization. The two estimates thus seem inconsistent and we conclude that the magnitude of this subsurface overturning remains unknown.

But, clearly, dense waters in the Greenland Sea basin extend well above the height of the JMK Ridge. Therefore, in addition to possible ageostrophic flows through gaps in the ridge system (e.g. Østerhus and Gammelsrød, 1999), baroclinic instability of the front above the ridge is a mechanism by which dense water *should* enter into the eastern basins. An unexplored scenario is that the required mixing for transformation to lighter waters in the east stems not from the background internal wave field but from enhanced mixing during winter months. In principle it is at least possible that some of the very dense water is entrained up during the deepest convection events in winter. Leaving details of this scenario for future studies, we note in closing that Ito and Marshall (2008) have also reported evidence for such a mixing-driven subsurface overturning cell in the Southern Ocean.

Obviously our estimates of the eddy-induced overturning circulation suffer from shortcomings of the eddy parameterization used. We have used a state-of-the-art parameterization,

but this too is a very crude model of actual mesoscale eddy transport. The results obtained rely on free parameters that deserve more careful calibration than attempted here. Our treatment of eddy fluxes near the sea surface and ocean bottom was rudimentary and we also had to introduce depth-decaying eddy diffusivities to avoid unreasonably large transport values at high densities. Our ad hoc introduction of depth-dependent diffusivities is far from rigorous, but the results produced were in qualitative agreement with other studies that have pointed to the existence of depth-decaying diffusivities. Surface intensified eddy diffusivities may be due to steep topography influencing Eady instability by radiating eddy kinetic energy away at depth (Treguier and McWilliams, 1990; LaCasce and Brink, 2000) or, alternatively, they may simply reflect the presence of surface-trapped ageostrophic instability working to overturn the surface mixed layer alone (Boccaletti *et al.*, 2007).

Despite its many obvious shortcomings, and save for the unresolved issue of a possible subsurface, mixing-driven, overturning cell, the eddy parameterization did a fair job at reproducing the shape of the air–sea transformation curves seen here. The good match supports our prior expectations that the buoyancy and heat transport between the boundary current and the interior regions within the Nordic Seas is dominated not by Eulerian mean currents but by the eddy-induced velocity. In this respect the situation at high northern latitudes is somewhat different from that in the Southern Ocean. In the south, eddies are directly responsible for the actual poleward oceanic transport of heat, while in the north the presence of the continents allows boundary currents to mediate the bulk of the meridional transport. But, as seen here, the eddies play a crucial role in the north as well since they effectively spread out the warm water and so enlarge the area over which it is exposed to the cold atmosphere. The effect on the ocean circulation itself and even the hemispheric meridional temperature contrast should not be underestimated. By enhancing the total buoyancy loss experienced by the boundary currents, lateral eddy fluxes also enhance the large-scale baroclinic pressure gradients that drive these same currents and the heat transport from the south.

Acknowledgments. We would like to thank two anonymous reviewers for very useful comments and suggestions. This work was partially conducted under the POCAHONTAS project (178345/S30) funded by the Norwegian Research Council.

APPENDIX A

A 0.5° × 0.25° gridded hydrography of the Nordic Seas

To make accurate estimates of thermal wind currents in and out of our study regions we made a gridded hydrographic data set for the Nordic Seas using Hydrobase2 software (HB2: Curry, 1996, 2001). Wishing to capture more detail than what is present in the $1^\circ \times 1^\circ$ resolution of the World Ocean Atlas (WOA09; Antonov *et al.*, 2010; Locarnini *et al.*, 2010), we opted for a monthly product on a $0.5^\circ \times 0.25^\circ$ longitude-latitude grid, or approximately 30 km nominal resolution (isotropic at 60°N).

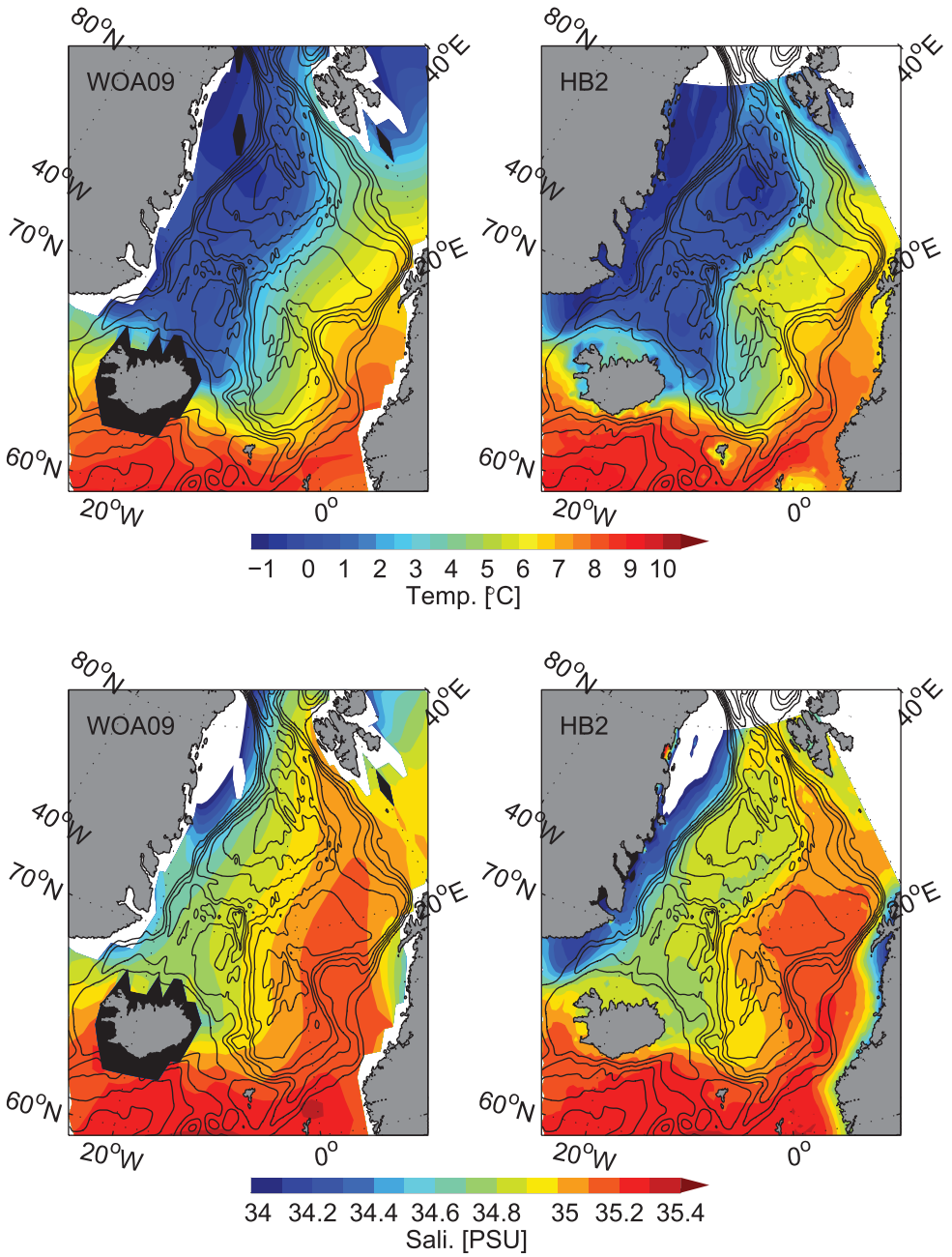

Figure 10. Annual-mean (top) temperature and (bottom) salinity at 100 m depth for (left) WOA09 and (right) the new "HB2" climatology.

Hydrographic station data come from NODC's World Ocean Database, WOCE Hydrographic Programme, NSIDC (Joint U.S. / Russian Atlas of the Arctic Ocean), ICES, BarKode (Barents and Kara Seas Oceanographic Database) and various other sources. With Hydrobase2 the objective mapping is conducted on isopycnal surfaces (with gradual tapering to geopotential surfaces near the sea surface). The procedure is thus comparable to that used by Rossby *et al.* (2009) and results in a hydrographic climatology of the Nordic Seas where the creation of artificial water masses from the horizontal averaging procedure is kept to a minimum.

Here we constructed one gridded field for each month. Because of the sparsity of deep observations an initial guess based on data from all seasons was made below 200 meters, but enhanced weight were given to observations of the correct month. Objective mapping to the regular grid, made on a set of pre-defined isopycnals, was made with a Gaussian kernel with e-folding scale of 56 km. After initial gridding any remaining data gaps were filled by interpolation using the same type of Gaussian kernel, and finally the complete field was smoothed with a 9-point boxcar filter. After this smoothing the effective horizontal resolution is 50–70 km. The final product was finally mapped from isopycnals to a regular geopotential grid in the vertical.

Figure 10 shows annual mean temperature and salinity at 100 m depth from WOA09 and from the new HB2 climatology. The two products agree in the positioning and property magnitude of the large-scale fields; there is cold and fresh water of polar origin dominating west of the Jan Mayen-Mohn-Knipovich Ridge system and warm and salty water of Atlantic origin dominating in the east. But the added resolution and the isopycnal averaging procedure of the HB2 climatology do result in a more accurate picture of finer details. In particular, the new climatology better captures the strong topographic constraints on tracer fields, as seen e.g. in the positioning of the polar front along the JMK Ridge and the Atlantic Water core along the continental slope in the east.

APPENDIX B

Eddy transport in a primitive equation channel model

We test some aspects of eddy fluxes and the parameterization of these in primitive equation simulations of an idealized channel consisting of a continental shelf connected to the deep ocean via a linear continental slope. Flow in the channel is driven by heating through the sea bed at the inner region of the continental shelf and by cooling through the sea surface (by relaxation to a fixed atmospheric temperature). The baroclinicity caused by the uneven temperature distribution in the model sets up thermal wind currents along the channel (Fig. 11). Cross-channel heat transport, however, is primarily due to baroclinic instability and eddy transport.

The simulations, described in detail in Isachsen (2011), were done with the ROMS model (Shchepetkin and McWilliams, 2005) at 4 km horizontal resolution. Analysis of the model hydrography showed that the model typically resolved the fastest-growing Eady wave with

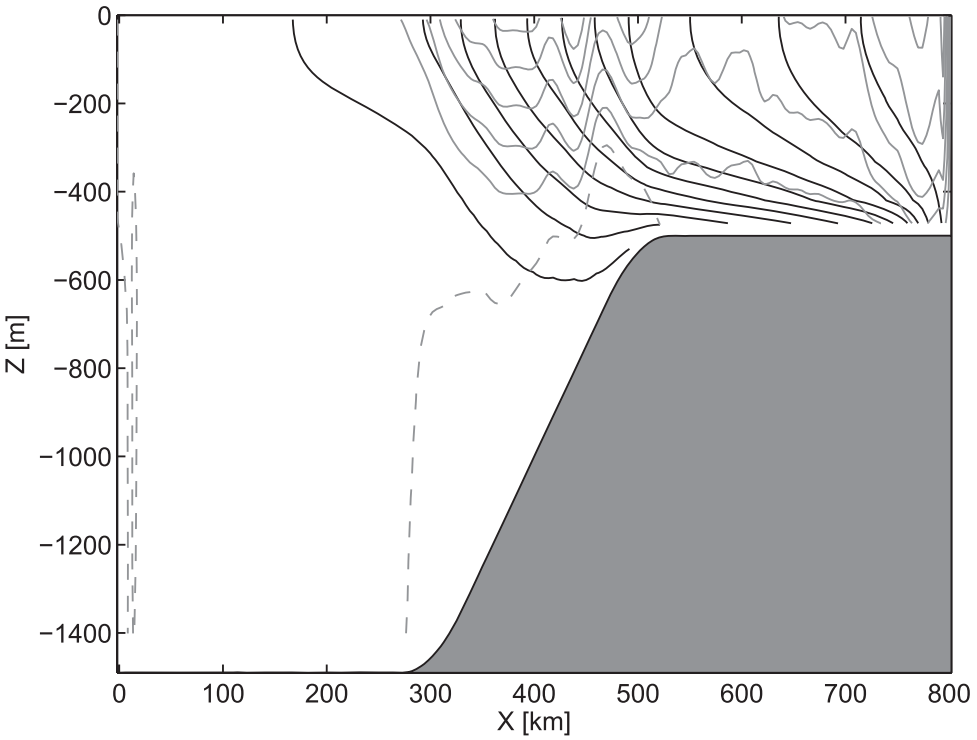

Figure 11. Time-mean fields of an idealized channel simulation with a continental slope of steepness $2.5 \cdot 10^{-3}$: (black lines) density field and (gray lines) thermal wind currents relative to the bottom. The contour interval is $0.05\,\mathrm{kg\,m^{-3}}$ for density and $0.01\,\mathrm{m\,s^{-1}}$ for velocity.

five horizontal grid points or more. After a 5000 day spin-up period, the model horizontal eddy density transport $\overline{u'\rho'}$ near the sea surface (primes indicating perturbations from the time mean and the overbar representing both the time mean and an average along the channel length) was diagnosed over a period of 1000 days. Horizontal eddy diffusivities were then calculated as $\kappa = -\overline{u'\rho'}/\overline{\rho}_x$, where $\overline{\rho}_x$ is the horizontal gradient of the time-mean density field.

As in the main text, parametrized density transports were made with three different forms for diffusivities. First, we simply use a constant diffusivity taking on the canonical value

$$\kappa_c = 1000\,\mathrm{m^2 s^{-1}}. \tag{35}$$

Secondly, we use a diffusivity proportional to the top-to-bottom thermal wind shear V_{tw} and the first internal deformation radius L_d (Stone, 1972),

$$\kappa_S = \alpha_S V_{tw} L_d, \tag{36}$$

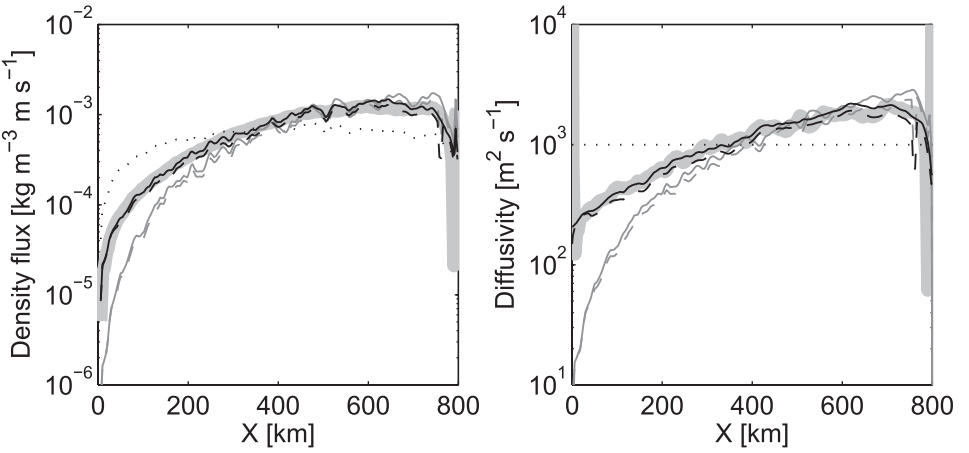

Figure 12. Surface (left) density fluxes and (right) diffusivities for a simulation with a flat bottom. Shown are the results (thick gray lines) diagnosed from the model and for a down-gradient parameterization with different diffusivities: (dotted lines) constant diffusivity, (thin gray lines) Stone (1972) diffusivities, and (thin black lines) Holloway (1986) diffusivities. The dashed gray and black lines show the results when the kinematic suppression suggested by Ferrari and Nikurashin (2010) is included.

Finally, we use a diffusivity proportional to the model RMS sea surface height η' (Holloway, 1986),

$$\kappa_H = \alpha_H \frac{g}{f} (\overline{\eta'^2})^{1/2}. \tag{37}$$

Results presented here use tuning parameters $\alpha_S = 25$ and $\alpha_H = 0.8$ and are based on two different geometries, one without a continental slope at all (i.e. a flat bottom simulation; Fig. 12) and one with a slope of steepness $5 \cdot 10^{-3}$ (Fig. 13).

As the water in the channel gets gradually cooler away from the heating region, the surface buoyancy loss and the compensating horizontal density transport also fall off. More interestingly, the diagnosed eddy diffusivity also falls off away from the heating region, so the parametrized buoyancy transport with constant diffusivities is typically too low near the heating region and typically too high far away. The classical Stone (1972) scaling for diffusivities, by the total thermal wind shear and the first internal deformation radius, does a better job for the flat-bottom simulation (Fig. 12). But the actual (diagnosed) diffusivities far from the heating region are higher than in Stone's model, an indication that non-local sources of eddy kinetic energy, i.e. advection of EKE, may be important. For this same flat bottom case, the diffusivity estimated from the model's sea surface variability (Holloway, 1986) is extremely close to the diagnosed diffusivity. And so is the parametrized buoyancy transport.

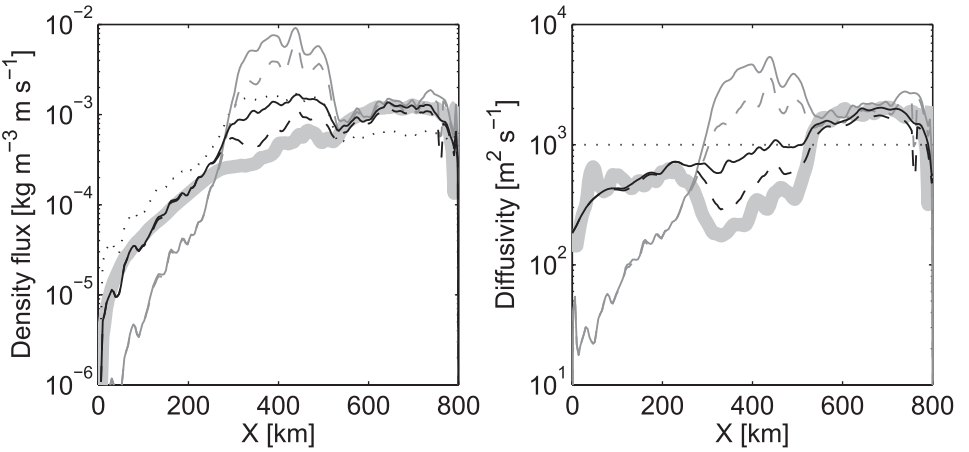

Figure 13. Same as Fig. 12 but for a simulation with a bottom slope of $5 \cdot 10^{-3}$ in the center of the channel (as in Fig. 11).

The addition of a topographic slope has a considerable impact on the eddy dynamics in the model, and the diagnosed diffusivities drop by nearly an order of magnitude in the slope region itself (Fig. 13). As argued by Blumsack and Gierasch (1972) and Mechoso (1980), the slope both reduces the growth rates and the length scale of unstable Eady waves—relative to the flat bottom case. And yet the actual transport over the slope is almost unchanged. The likely explanation is that the reduced eddy transport efficiency leads to stronger baroclinicity over the slope (Fig. 11), thus increasing both the thermal wind shear and the deformation radius to effectively compensate for the suppressing effect of the slope. The Stone parameterization, sensitive to the increased baroclinicity *but not* to the suppression by the slope, therefore overestimates the diffusivity and the transport considerably. The Holloway estimate does considerably better since the RMS SSH field contains some information about the reduced kinetic energy levels and length scales over the slope (relative to the flat bottom case). But this expression also overestimates diffusivities and transport somewhat.

Figure 11 shows that a baroclinic jet forms over the slope region. We therefore also tested the kinematic suppression factor proposed by Ferrari and Nikurashin (2010),

$$\kappa_{eff} = \frac{\kappa}{1 + d_2 V_0^2 / EKE},$$

where κ is the diffusivity in the absence of mean flow, V_0 is the mean current speed and EKE is eddy kinetic energy. For the channel simulations studied here we found that setting tuning parameter $d_2 = 2$ gave a sensible compromise between desired suppression over the slope region and unwanted suppression elsewhere. Stone diffusivities were still unrealistically high over the slope region, but Holloway diffusivities could now be brought reasonably well in line with the actual diffusivities and transport in the model (Fig. 13).

REFERENCES

Aaboe, S. and O. A. Nøst. 2008. A diagnostic model of the Nordic Seas and Arctic Ocean circulation: Quantifying the effects of a variable bottom density along a sloping bottom. J. Phys. Oceanogr., *38*, 2685–2703.

Abernathey, R., J. Marshall, M. Mazloff, and E. Schuckburgh. 2010. Enhancement of mesoscale eddy stirring at steering levels in the Southern Ocean. J. Phys. Oceanogr., *40*, 170–184.

Aiki, H., T. Jacobson, and T. Yamagata. 2004. Parameterizing ocean eddy transports from surface to bottom. Geophys. Res. Let., *31* (L19302).

Andersson, M., J. H. LaCasce, K. J. Orvik, I. Koszalka, and C. Mauritzen. 2011. Variability of the Norwegian Atlantic Current and associated eddy field from surface drifters. J. Geophys. Res., *116*, C08032, doi:10.1029/2011JC007078.

Antonov, J. I., D. Seidov, T. P. Boyer, R. A. Locarnini, A. V. Mishonov, H. E. Garcia, O. K. Baranova, M. M. Zweng, and D. R. Johnson. 2010. World Ocean Atlas 2009, Volume 2: Salinity. Technical report, Salinity. S. Levitus, ed., NOAA Atlas NESDIS 69, U.S. Government Printing Office, Washington, D.C., 184 pp.

April 2011. SSALTO/DUACS User Handbook. AVISO, 2rev, 5th ed. CLS-DOS-NT-06-034.

Blumsack, S. L. and P. J. Gierasch. 1972. Mars: The effects of topography on baroclinic instability. J. Atmos. Sci., *29*, 1081–1089.

Boccaletti, G., R. Ferrari, and B. Fox-Kemper. 2007. Mixed layer instabilities and restratification. J. Phys. Oceanogr., *37*, 2228–2250.

Cerovečki, I. and J. Marshall. 2008. Eddy modulation of air-sea interaction and convection. J. Phys. Oceanogr., *38*, 65–83.

Curry, R. G. 1996. A database of hydrographic stations and tools for climatological analysis. Technical report, Woods Hole Oceanographic Institution, Woods Hole, MA.

—— 2001. Hydrobase 2: A database of hydrographic stations and tools for climatological analysis. Technical report, Woods Hole Oceanographic Institution, Woods Hole, MA.

Danabasoglu, G. and J. Marshall. 2007. Effects of vertical variations of thickness diffusivity in an ocean general circulation model. Ocean Model., *18*, 122–141.

Davis, R. E., R. de Szoeke, R. Halpern, and P. Niiler. 1981. Variability in the upper ocean during MILE. Part I: The heat and momentum balances. Deep-Sea Res., *28*, 1427–1452.

Dee, D. P. *et al.* 2011. The ERA-Interim reanalysis: configuration and performance of the data assimilation system. Quart. J. Roy. Met. Soc., *137*, 553–597.

de Szoeke, R. A. and M. D. Levine. 1981. The advective flux of heat by mean geostrophic motions in the Southern Ocean. Deep-Sea Res., *28*, 1057–1085.

Döös, K. and D. Webb. 1994. The Deacon Cell and other meridional cells of the Southern Ocean. J. Phys. Oceanogr., *24*, 429–442.

Eden, C. 2011. A closure for meso-scale eddy fluxes based on linear instability theory. Ocean Model., *38*, 362–369.

Eden, C., M. Jochum, and G. Danabasoglu. 2009. Effects of different closures for thickness diffusivity. Ocean Model., *26*, 47–59.

Fahrbach, E., J. Meincke, S. Østerhus, G. Rohardt, U. Schauer, V. Tverberg, and J. Verduin. 2001. Direct measurements of volume transports through Fram Strait. Polar Res., *20*, 217–224.

Ferrari, R., S. M. Griffies, A. G. Nurser, and G. K. Vallis. 2010. A boundary-value problem for the parameterized mesoscale eddy transport. Ocean Model., *32*, 143–156.

Ferrari, R. and M. Nikurashin. 2010. Suppression of eddy diffusivity across jets in the Southern Ocean. J. Phys. Oceanogr., *40*, 1501–1519.

Ferrari, R., J. C. McWilliams, V. M. Canuto, and M. Dubovikov. 2008. Parameterizing eddy fluxes near oceanic boundaries. J. Phys. Oceanogr., *21*, 2770–2789.

Ferreira, D., J. Marshall, and P. Heimbach. 2005. Estimating eddy stresses by fitting dynamics to observations using a residual-mean ocean circulation model and its adjoint. J. Phys. Oceanogr., *35*, 1891–1910.

Fox-Kemper, B., G. Danabasoglu, R. Ferrari, S. M. Griffies, R. W. Hallberg, M. M. Holland, M. E. Maltrud, S. Peacock, and B. L. Samuels. 2011. Parameterization of mixed layer eddies. III: Implementation and impact in global ocean climate simulations. Ocean Model., *39*, 61–78.

Ganachaud, A. and C. Wunsch. 2003. Large scale ocean heat and freshwater transports during the World Ocean Circulation Experiment. J. Climate, *16*, 696–705.

Garrett, C. and A. Tandon. 1997. The effects on water mass formation of surface mixed layer time-dependence and entrainment fluxes. Deep-Sea Res., *44*, 1991–2006.

Gent, P. R. and J. C. McWilliams. 1990. Isopycnal mixing in ocean circulation models. J. Phys. Oceanogr., *20*, 150–155.

Gent, P. R., J. Willebrand, T. J. McDougall, and J. C. McWilliams. 1995. Parameterizing eddy-induced tracer transports in ocean circulation models. J. Phys. Oceanogr., *25*, 463–474.

Green, J. S. A. 1970. Transfer properties of the large-scale eddies and the general circulation of the atmosphere. Quart. J. Roy. Met. Soc., *96*, 157–185.

Griffies, S. M. 2004. Fundamentals of Ocean Climate Models, Princeton University Press.

Holloway, G. 1986. Estimation of oceanic eddy transports from satellite altimetry. Nature, *323*, 243–244.

Holloway, G. and S. S. Kristmannsson. 1984. Stirring and transport of tracer fields by geostrophic turbulence. J. Fluid Mech., *141*, 27–50.

Isachsen, P. E. 2011. Baroclinic instability and eddy tracer transport across sloping bottom topography: How well does a modified Eady model do in primitive equation simulations? Ocean Model., *39*, 183–199.

Isachsen, P. E., J. H. LaCasce, C. Mauritzen, and S. Häkkinen. 2003. Wind-driven variability of the large-scale recirculation flow in the Nordic Seas and the Arctic Ocean. J. Phys. Oceanogr., *33*, 2434–2550.

Isachsen, P. E., J. H. LaCasce, and J. Pedlosky. 2007a. Rossby wave instability and apparent phase speeds in large ocean basins. J. Phys. Oceanogr., *37*, 1177–1191.

Isachsen, P. E., C. Mauritzen, and H. Svendsen. 2007b. Dense water formation in the Nordic Seas diagnosed from sea surface buoyancy fluxes. Deep-Sea Res., *54*, 22–41.

Ito, T. and J. Marshall. 2008. Control of lower-limb overturning circulation in the Southern Ocean by diapycnal mixing and mesoscale eddy transfer. J. Phys. Oceanogr., *38*, 2832–2845.

Kalnay, E., M. Kanamitsu, R. Kistler, W. Collins, D. Deaven, L. Gandin, M. Iredell, S. Saha, G. White, J. Woollen, Y. Zhu, M. Chelliah, W. Ebisuzaki, W. Higgins, J. Janowiak, K. Mo, C. Ropelewski, J. Wang, A. Leetmaa, R. Reynolds, R. Jenne, and D. J. D. 1996. The NCEP/NCAR 40-year reanalysis project. Bull. Amer. Met. Soc., *77*, 437–471.

Karsten, R. H. and J. Marshall. 2002. Constructing the residual circulation of the ACC from observations. J. Phys. Oceanogr., *32*, 3315–3327.

Keffer, T. and G. Holloway. 1988. Estimating Southern Ocean eddy flux of heat and salt from satellite altimetry. Nature, *332*, 624–626.

Killworth, P. D. 1997. On the parameterization of eddy transfer. part I. theory. J. Mar. Res., *55*, 1171–1197.

Köhl, A. 2007. Generation and stability of a quasi-permanent vortex in the Lofoten Basin. J. Phys. Oceanogr., *37*, 2637–2651.

Koszalka, I., J. H. LaCasce, M. Andersson, K. A. Orvik, and C. Mauritzen. 2011. Surface circulation in the Nordic Seas from clustered drifters. Deep-Sea Res. I, *58*, 468–485.

LaCasce, J. H. and K. H. Brink. 2000. Geostrophic turbulence over a slope. J. Phys. Oceanogr., *30*, 1305–1324.

LaCasce, J. H. and J. Pedlosky. 2004. The instability of Rossby basin modes and the oceanic eddy field. J. Phys. Oceanogr., *34*, 2027–2041.

Large, W., G. Danabasoglu, S. Doney, and J. C. McWilliams. 1997. Sensitivity to surface forcing and boundary layer mixing in a global ocean model: Annual-mean climatology. J. Phys. Oceanogr., *27*, 2418–2447.

Large, W. G. and A. J. Nurser. 2001. Ocean Circulation and Climate, Volume 77 of International Geophysics Series, Ocean surface water mass transformation, Academic Press, NY, 317–336.

Le Sommer, J., F. d'Ovidio, and G. Madec. 2011. Parameterization of subgrid stirring in eddy resolving ocean models. Part 1: Theory and diagnostics. Ocean Model., *39*, 154–169.

Locarnini, R. A., A. V. Mishonov, J. I. Antonov, T. P. Boyer, H. E. Garcia, O. K. Baranova, M. M. Zweng, and D. R. Johnson. 2010. World Ocean Atlas 2009, Volume 1: Temperature. Technical report, S. Levitus, ed., NOAA Atlas NESDIS 68, U.S. Government Printing Office, Washington, D.C., 184 pp.

Marshall, J., D. Jamous, and J. Nilsson. 1999. Reconciling thermodynamic and dynamic methods of computation of water-mass transformation rates. Deep-Sea Res. I, *46*, 545–572.

Marshall, J. and T. Radko. 2003. Residual-mean solutions for the Antarctic Circumpolar Current and its associated overturning circulation. J. Phys. Oceanogr., *33*, 2341–2354.

Mauritzen, C. 1996. Production of dense overflow waters feeding the North Atlantic across the Greenland-Scotland Ridge. Part 1: Evidence for a revised circulation scheme. Deep-Sea Res. I, *43*, 769–806.

McDougall, T. J. and P. C. McIntosh. 2001. The temporal-residual-mean velocity. Part II: Isopycnal interpretation and the tracer and momentum equations. J. Phys. Oceanogr., *31*, 1222–1246.

Mechoso, C. R. 1980. Baroclinic instability of flows along sloping boundaries. J. Atmos. Sci., *37*, 1393–1399.

Naveira Garabato, A. C., K. I. C. Oliver, A. J. Watson, and M. J. Messias. 2004. Turbulent diapycnal mixing in the Nordic Seas. J. Geophys. Res., *109* (C12010). doi:0.1029/2004JC002411.

Nilsson, J., G. Walin, and G. Brostrøm. 2005. Thermohaline circulation induced by bottom friction in sloping-boundary basins. J. Mar. Res., *63*, 705–728.

Nøst, O. A. and P. E. Isachsen. 2003. The large-scale time-mean ocean circulation in the Nordic Seas and the Arctic Ocean estimated from simplified dynamics. J. Mar. Res., *61*, 175–210.

Nurser, A. J. G., R. Marsh, and R. G. Williams. 1999. Diagnosing water mass formation from air-sea fluxes and surface mixing. J. Phys. Oceanogr., *29*, 1468–1487.

Olbers, D. and M. Visbeck. 2005. A model of the zonally averaged stratification and overturning in the Southern Ocean. J. Phys. Oceanogr., *37*, 1190–1205.

Osborn, T. R. 1980. Estimates of the local rate of vertical diffusion from dissipation measurements. J. Phys. Oceanogr., *10*, 83–89.

Østerhus, S. and T. Gammelsrød. 1999. The abbyss of the Nordic Seas is warming. J. Climate, *12*, 3297–3304.

Pedlosky, J. and M. Spall. 2005. Boundary intensification of vertical velocity in a beta-plane basin. J. Phys. Oceanogr., *35*, 2487–2500.

Price, J. F., R. A. Weller, and R. R. Schudlich. 1987. Wind-driven ocean currents and Ekman transport. Science, *238*, 1534–1538.

Rossby, T., V. Ozhigin, V. Ivshin, and S. Bacon. 2009. An isopycnal view of the Nordic Seas hydrography with focus on properties of the Lofoten Basin. Deep-Sea Res., *56*, 1955–1971.

Schott, F. and H. Stommel. 1978. Beta-spirals and absolute velocities in diffferent oceans. Deep-Sea Res., *25*, 961–1010.

Schott, F. and R. Zantopp. 1980. On the effect of vertical mixing on the determination of absolute currents by the beta spiral method. Deep-Sea Res., *27*, 173–180.

Segtnan, O. H., T. Furevik, and A. D. Jenkins. 2011. Heat and freshwater budgets of the Nordic Seas computed from atmospheric reanalysis and direct ocean observations. J. Geophys. Res., *116* (C11003). doi:10.1029/2011JC006939.

Shchepetkin, A. F. and J. McWilliams. 2005. The Regional Oceanic Modeling System: A split-explicit, free-surface, topography-following-coordinate ocean model. Ocean Model., *9*, 347–404.

Smith, K. S. and J. Marshall. 2009. Evidence for enhanced eddy mixing at middepth in the Southern Ocean. J. Phys. Oceanogr., *39*, 50–69.

Sommer, J. L., F. D'Ovidio, and G. Madec. 2011. Parameterization of subgrid stirring in eddy resolving ocean models. Part 1: Theory and diagnostics. Ocean Model., *39*, 154–169.

Spall, M. A. 2004. Boundary currents and water mass transformation in marginal seas. J. Phys. Oceanogr., *34*, 1197–1213.

—— 2005. Buoyancy-forced circulations in shallow marginal seas. J. Mar. Res., *63*, 729–752.

—— 2010a. Dynamics of downwelling in an eddy-resolving convective basin. J. Phys. Oceanogr., *40*, 2341–2347.

—— 2010b. Non-local topographic influences on deep convection: An idealized model for the Nordic Seas. Ocean Model., *32*, 72–85.

Spall, M. A. and D. C. Chapman. 1998. On the efficiency of baroclinic eddy heat transport across narrow fronts. J. Phys. Oceanogr., *28*, 2275–2287.

Spall, M. A. and R. S. Pickart. 2001. Where does dense water sink? a Subpolar Gyre example. J. Phys. Oceanogr., *31*, 810–826.

Speer, K. G. 1997. A note on average cross-isopycnal mixing in the North Atlantic Ocean. Deep-Sea Res., *44*, 1981–1990.

Stone, P. H. 1972. On non-geostrophic baroclinic instability: Part III. The momentum and heat transports. J. Atmos. Sci., *29*, 419–426.

Straneo, F. 2006a. Heat and freshwater transport through the Central Labrador Sea. J. Phys. Oceanogr., *36*, 606–628.

—— 2006b. On the connection between dense water formation, overturning, and poleward heat transport in a convective basin. J. Phys. Oceanogr., *36*, 1822–1840.

Tandon, A. and L. Zhao. 2004. Mixed layer transformation for the North Atlantic for 1990-2000. J. Geophys. Res., *109* (C5018). doi:10.1029/2003JC002059.

Treguier, A. M. and J. C. McWilliams. 1990. Topographic influences on wind-driven, stratified flow in a beta-plane channel: An idealized model for the Antarctic Circumpolar Current. J. Phys. Oceanogr., *20*, 321–343.

Venaille, A., G. K. Vallis, and K. Shafer Smith. 2011. Baroclinic turbulence in the ocean: analysis with primitive equation and quasigeostrophic simulations. J. Phys. Oceanogr., *41*, 1605–1623.

Walin, G. 1982. On the relation between sea-surface heat flow and thermal circulation in the ocean. Tellus, *34*, 187–195.

Walin, G., G. Brostrøm, J. Nilsson, and O. Dahl. 2004. Baroclinic boundary currents with downstream decreasing buoyancy: A study of an idealized Nordic Seas system. J. Mar. Res., *62*, 517–543.

Wunsch, C. 1996. The Ocean Circulation Inverse Problem. Cambridge University Press.

Yim, B. Y., Y. Noh, B. Qui, S. H. You, and J. H. Yoon. 2010. The vertical structure of eddy heat transport simulated by an eddy-resolving OGCM. J. Phys. Oceanogr., *41*, 340–353.

Received: *2 May, 2011*; revised: *13 January, 2012*.